SLAC–PUB–4428
September 1987
(E)

Experimental Results on QCD from e^+e^- Annihilation*

W. DE BOER†

Max–Planck–Institut für Physik und Astrophysik,
Werner–Heisenberg–Institut für Physik, D 8000 Munich 40
and
Stanford Linear Accelerator Center,
Stanford University, Stanford, CA 94305

Contents

* Work supported in part by the Department of Energy, Contract DE–AC03–76SF00515.

† Mailing address: SLAC (Bin 61), P. O. Box 4349, Stanford, CA 94305, USA
Bitnet address: user WDB at node SLACVM

Invited talk at the Xth WARSAW Symposium on Elementary Particle Physics, Kazimierz, Poland, May 25–29, 1987

Abstract

A review is given on QCD results from studying e^+e^- annihilation with the PEP and PETRA storage rings with special emphasis on jet physics and the determination of the strong coupling constant α_s.

1 Introduction

This paper reviews the progress on the theory of hadronic interactions during the eight years of PEP and PETRA physics. This is an appropriate time, since a new generation of e^+e^- storage rings is underway (SLC and LEP) or ready (TRISTAN), which will extend the maximium centre of mass energies reached sofar to the Z^0 mass and beyond, thus opening a whole new field of physics. I will restrict myself to results from hadronic events from e^+e^- annihilation and neglect QCD results from two photon physics. The emphasis will be on newer results about the determination of the strong coupling constant, since other topics, like searches for new phenomena, jet properties, heavy quark fragmentation, and gluon fragmentation have been discussed in detail elsewhere [1].

In order to appreciate how much progress was made, let us review what was known some 10 years ago[2] :

- In 1972 Quantum Chromodynamics (QCD) was proposed by Fritzsch and Gell-Mann[3] as a gauge invariant field theory of the strong interactions: the gauge bosons are 8 coloured gluons, which are responsible for the strong forces between the quarks very much like the exchange of photons yields the electromagnetic force between charged particles.

- QCD was given an enormous boost by the discovery of asymptotic freedom by Gross and Wilczek[4] and Politzer[5], the subsequent observation of scale invariance which offers a justification for the highly successful quark parton model (QPM), and the observation of logarithmic deviations from this invariance as predicted by QCD.

- The discovery of the J/Ψ in 1974 at SLAC[6] and Brookhaven[7] and the proof that it corresponded to a bound state of $c\bar{c}$ quarks completed the quark picture and left little doubt to the idea that the mathematical objects originally proposed by Gell-Mann[8] and Zweig[9] to classify the hadrons were real, existing quarks.

- The charmed quark fitted beautifully into the $SU(2) \otimes U(1)$ unified theory of the electroweak interactions, proposed by Glashow, Salam and Weinberg[10] and proven to be renormalizible by 't Hooft[11], since in this model the matter fields are arranged in left-handed doublets and right-handed singlets, so there was an 'empty' slot in the doublet structure of this so-called Standard Model for the charmed quark. Actually from the absence of stangeness changing

neutral currents Glashow, Iliopoulos and Maiani (GIM) had predicted the existence of the charmed quark[12].

- After 1974 a new heavy lepton (called τ) with its own neutrino was discovered by Perl and collaborators at SLAC[14] and a new quark (called bottom) was discovered by Lederman's group at Fermilab[13]. Given the succes of the Standard Model, one was in the same situation of having an 'empty' slot for a new quark (called top) in a thirth generation of quarks and leptons. So by the time of proposal writing for the PETRA experiments the quark picture was well established and the detectors were all optimized to do 'top' physics.

However, what was going to be one of the major discoveries at PETRA, namely the discovery of the gluon, was not even considered in the proposals as a physics topic. The main reason is that jet physics at that time was not very advanced, for the simple reason that the jet energies were too small to see jets on an event by event basis, so the idea that one might observe gluons as jets was not obvious, although it was proposed by several theorists[15]. The main evidence for jets in e^+e^- annihilation at that time came from the MARK-I Collaboration[16], who observed a deviation of the sphericity of hadronic events from phase space. Furthermore, the beams at SPEAR turned out to be polarized, which yielded an azimuthal variation of the sphericity axis, as expected for spin 1/2 quarks.

The outline of this paper is as follows:

- After summarizing the predictions of the Standard Model we discuss the main features of jet physics. We will be short, since this topic has been reviewed many times.
- We then proceed to the discussion of the more ambitious task of the determination of the strong coupling constant α_s. Note that within QCD the coupling between all quarks and gluons is supposed to be the same, so there is only one coupling constant to be determined.
- We conclude with a summary.

2 Standard Model Predictions

Even at present energies the effects of Z^0 exchange are noticeable, so one has to take the complete Standard Model of $SU(3)_C \otimes SU(2)_L \otimes U(1)$ into account. This model has 4 fundamental parameters (aside from masses and mixing angles) : three coupling constants for SU(3), SU(2) and U(1), respectively, and the vacuum expectation value of the Higgs doublet. If the model contains Higgs representations other than doublets, the theory has an additional parameter, usually parametrized by the ρ-parameter. To make comparisons with experiments easier, one should use parameters closely related to physical processes. Two of the parameters can be chosen as follows: the fine structure constant $\alpha = 1/137.036$ as obtained from the

Josephson effect, and the Fermi coupling constant $G_F = 1.16637\ 10^{-5}\mathrm{GeV}^{-2}$, as derived from the muon lifetime after applying the appropriate radiative corrections. As a third parameter one can take either mass of the neutral gauge boson M_Z or the electroweak mixing angle θ_W defined by $\cos\theta_W = M_W/M_Z$, where M_W is the mass of the charged gauge bosons. In both cases M_W is predicted in case $\rho = 1$, else one has to use $\cos\theta_W = M_W/(\rho M_Z)$. M_Z and θ_W are related via α and G_F by:

$$\frac{G_F(1-\triangle r)M_Z^2}{8\sqrt{2}\pi\alpha} = \frac{1}{16\sin^2\theta_W\cos^2\theta_W} \tag{1}$$

Here $\triangle r \approx 0.07$[17] are one-loop radiative corrections, which have not been absorbed in G_F. They depend on the unknown top- and Higgs mass. E.g. they vary from $\approx$7 % to 6 % (3%, 0%) for top masses varying from 45 GeV to 90 (180, 240) GeV and for a Higgs mass equal to the Z^0-mass. The fact that these corrections are so large comes mainly from the fact that α has been renormalized at low energy and its value increases by about 7% if it is calculated at the W-mass.

Of course, one could use different choices of parameters, e.g. M_W, but experimentally the previous choices can be better determined. The fourth parameter is either the value of the running strong coupling constant α_s at a given energy or the QCD scale parameter Λ, which determines the running of α_s and can be used to calculate α_s for a given energy.

2.1 Lowest order predictions

From the Feynman diagram for the production of quarks, as shown in Fig. 1a, one obtains the lowest order differential cross-section for the production of a pair of quarks with charge e_q:

$$\frac{d\sigma}{d\Omega}(e^+e^- \to q\bar{q}) = N_c e_e^2 e_q^2 \frac{\alpha^2}{4s}\beta(1+\cos^2\theta + (1-\beta^2)\sin^2\theta) \tag{2}$$

where θ is the scattering angle between the e^+ and the quark, and $\beta = \sqrt{1-4m_q^2/s}$ is the quark velocity. N_c=3 is the colour factor. Evidence for the colour of quarks comes from[2]:

- The Ω^- has spin 3/2 and is built up from three identical strange quarks. However, the Pauli principle does not allow spin 1/2 particles to be in the same state. To get the total wave function antisymmetric, one has to assume that each quark inside the Ω^- has an additional internal quantum number, called colour (red, green and blue quarks).
- The hadronic cross section of Eq. 2 would be a factor 3 too low compared with data, if the factor N_c was not introduced.
- The π^0 decays electromagnetically into two photons via a quark loop. Clearly the decay rate depends on the number of quarks in the loop and the experimentally observed decay rate requires N_c=3.

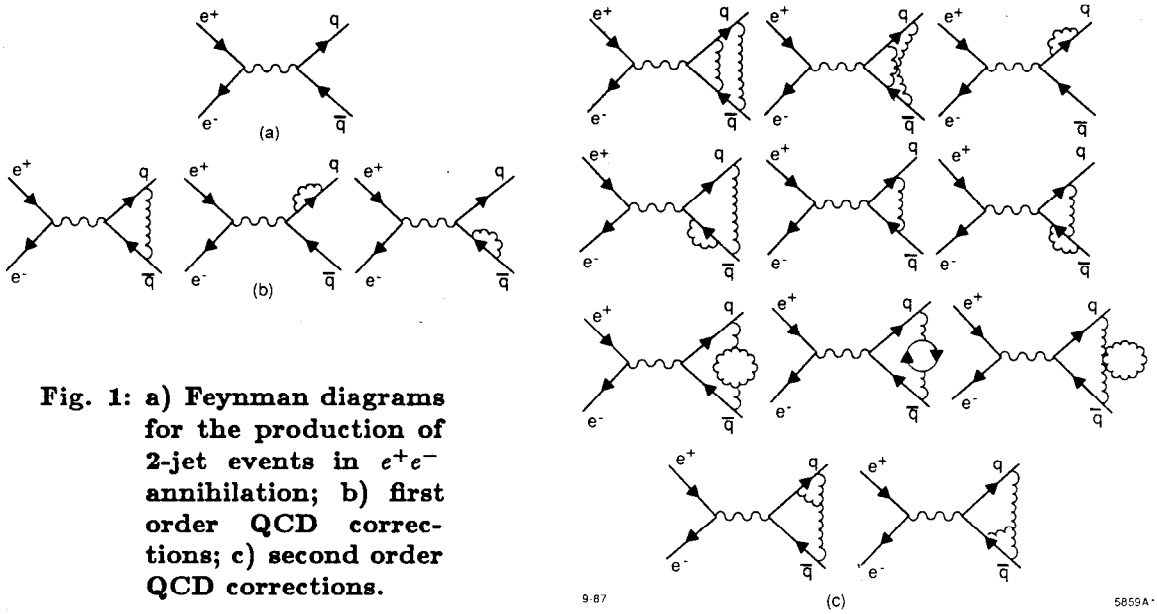

Fig. 1: a) Feynman diagrams for the production of 2-jet events in e^+e^- annihilation; b) first order QCD corrections; c) second order QCD corrections.

At higher energies the effect of the Z^0-exchange has to be included. In this case Eq. 2 becomes (if we use $\beta = 1$):

$$\frac{d\sigma}{d\cos\theta}(e^+e^- \rightarrow q\bar{q}) = N_c\frac{\pi\alpha^2}{2s}[C_1(1+\cos^2(\theta)) + C_2\cos(\theta)] \tag{3}$$

with

$$\begin{aligned} C_1 &= e_e^2e_q^2 + 2e_ee_qv_ev_q\Re(\chi) + (v_e^2+a_e^2)(v_q^2+a_q^2)|\chi|^2 \\ C_2 &= 4e_ee_qa_ea_q\Re(\chi) + 8v_ea_ev_qa_q|\chi^2| \end{aligned} \tag{4}$$

$$\begin{aligned} v_q &= 2(I_3^L + I_3^R) - 4\,e_q\sin^2\theta_W \\ a_q &= 2(I_3^L - I_3^R) \end{aligned} \tag{5}$$

and

$$\chi = \frac{\rho G_F}{8\sqrt{2}\pi\alpha}\,\frac{sM_Z^2}{s - M_Z^2 + i\sqrt{s}\Gamma_Z}\,\frac{1-\triangle r}{1-\triangle r'} \tag{6}$$

Here I_3^L and I_3^R are the 3th components of the weak isospin (see Table 1). In Eq. 6 the $1-\triangle r'$ term represents the loop corrections to the Z^0 propagator, while $1-\triangle r$ is defined by Eq. 1. Since $\triangle r' \approx \triangle r$ we can neglect both corrections in the fits to the hadronic cross section. Note that R-values are not corrected for $1-\triangle r'$, although asymmetry values are sometimes corrected for this factor in an indirect way[1]. In this case one has to apply only the correction factor $1-\triangle r$[18]. Then Eq. 6 becomes equal to its $\sin^2\theta_W$ parametrization (using Eq. 1):

$$\chi = \frac{G_F(1-\triangle r)}{8\sqrt{2}\pi\alpha}\,\frac{sM_Z^2}{s - M_Z^2 + i\sqrt{s}\Gamma_Z} \approx \frac{1}{16\sin^2\theta_W\cos^2\theta_W}\,\frac{s}{s - M_Z^2 + i\sqrt{s}\Gamma_Z} \tag{7}$$

[1]The loop corrections and the initial state radiative corrections for the Z^0-exchange have an opposite sign and are similar in magnitude at PETRA energies, so if one neglects them both, the remaining contribution is negligible[18] and one can forget about the $1-\triangle r'$ correction.

A summary about radiative corrections can be found in Ref.[19].

The terms proportional to $\Re(\chi)$ represent the interference between Z^0 and γ exchange and the terms proportional to $|\chi|^2$ the direct Z^0 exchange. The ratio of the total cross section contributions from Z^0 and γ exchange $((C_1 - e_f^2)/e_f^2)$ is shown in Table 1 for the various matter fields together with the coupling constants.

Fermion	I_3^L	I_3^R	a	v	e_f	$\frac{C_1-e_f^2}{e_f^2}$	A
neutrino	1/2	0	1	1	0	∞	0.12
μ, τ lepton	−1/2	0	−1	$-1 + 4\sin^2\theta_W = -0.08$	−1	1.2%	−0.15
u, c, t quarks	1/2	0	1	$+1 - \frac{8}{3}\sin^2\theta_W = 0.39$	+2/3	1.8%	−0.23
d, s, b quarks	−1/2	0	−1	$-1 + \frac{4}{3}\sin^2\theta_W = -0.69$	−1/3	11.0%	−0.41

Table 1: Summary of couplings and asymmetry for M_Z = 92 GeV and $\sin^2\theta_W$ = 0.23 at $\sqrt{s}$ = 44 GeV.

From Eq. 3 the total cross section is found to be $N_c C_1 4\pi\alpha^2/3s$ and the forward-backward asymmetry in the differential cross section equals:

$$A = \frac{\int_0^1 \frac{d\sigma}{d\cos\theta} d\cos(\theta) - \int_{-1}^0 \frac{d\sigma}{d\cos\theta} d\cos(\theta)}{\int_0^1 \frac{d\sigma}{d\cos\theta} d\cos(\theta) + \int_{-1}^0 \frac{d\sigma}{d\cos\theta} d\cos(\theta)} = \frac{3}{8}\frac{C_2}{C_1} \tag{8}$$

For leptonic final states the vector coupling v is small and only the interference term needs to be taken into account at PETRA energies. In this case the asymmetry in Eq. 8 depends only on the axial vector couplings. However, for quarks the vector couplings are large and the direct Z^0-exchange term ($\propto |\chi|^2$) is larger than the interference term at the highest PETRA energies.

2.2 First order QCD predictions

In first order the quark production is modified by gluon radiation as shown by the diagrams of Fig. 2a. The properties of the gluon are the following:

- the mass is 0.
- the spin parity $J^P = 0^-$.
- gluons are colour octet states. There exist $3N_c$ - 1 = 8 different gluons. At the gluon-quark vertex the colour of a quark is changed, e.g. a red-blue gluon g_{rb} transforms a red quark into a blue one. (see Fig. 3a).
- The gluon-quark coupling is independent of the colour and quark flavour, so it is the same for all quarks and gluons.
- In contrast to photons, which are electromagnetically neutral, gluons carry a colour charge. As a result, the gluons interact with themselves, which lead to the presence of three and four gluon vertices in the theory (see Fig. 3b).

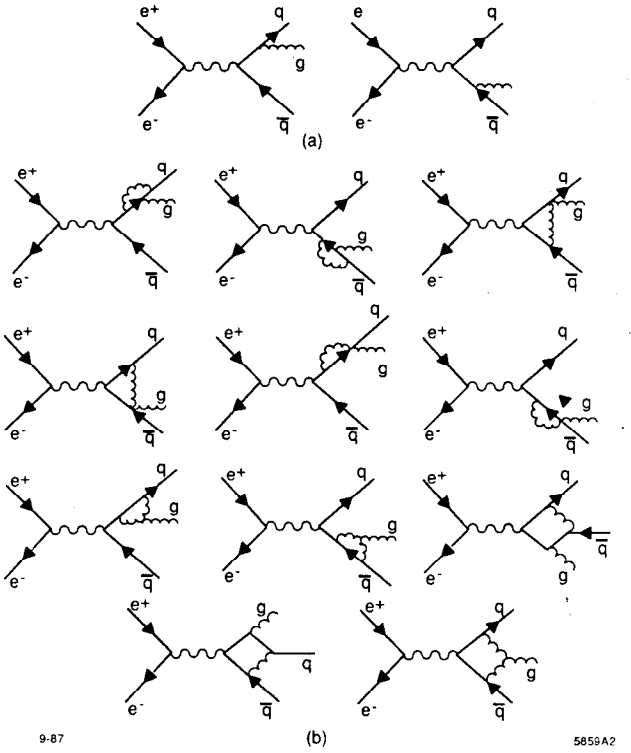

Fig. 2: a) Feynman diagrams for the production of 3-jet events in e^+e^- annihilation; b) second order QCD corrections.

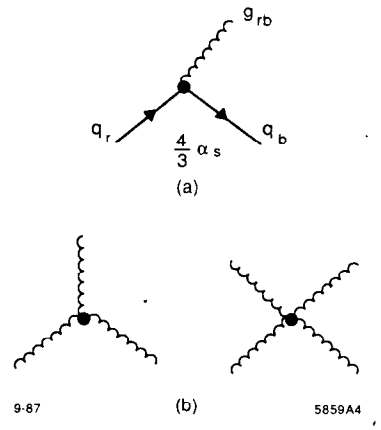

Fig. 3: a) Quark-gluon interaction: a red quark is transformed into a blue quark by emitting a red-blue gluon. The coupling strength=$4\alpha_s/3$.
b) Three - and four gluon vertices.

The differential cross section for gluon emission is given by[15]:

$$\frac{d^2\sigma(q\bar{q}g)}{\sigma(q\bar{q})dx_1dx_2} = \frac{\alpha_s}{2\pi}C_F\frac{x_1^2+x_2^2}{(1-x_1)(1-x_2)} = \frac{\alpha_s}{2\pi}C_F\left(\frac{y_{23}}{y_{13}}+\frac{2y_{12}}{y_{13}y_{23}}+\frac{y_{13}}{y_{23}}\right) \quad (9)$$

with 1, 2, 3 cyclic permutations. The Casimir operator $C_F = (N_c^2-1)/2N_c = 4/3$ for 3 colours and $x_i = E_i/E_{beam}$ are the fractional parton energies with $x_1+x_2+x_3 = 2$ and $y_{ij} = (p_i+p_j)^2/s$ are the scaled invariant masses; the subscripts 1 and 2 refer to the quarks and 3 to the gluon. This formula neglects quark masses, in which case $y_{ij} = (p_i+p_j)^2/s = 2p_ip_j/s = 1-x_k$ with i, j, and k cyclic permutations.

The coupling constant α_s between quarks and gluons determines the rate of gluon emission, which follows a typical bremsstrahlung spectrum: it diverges for soft gluons (x_1 and $x_2 \approx 1$, so double pole) and collinear gluons (x_1 or $x_2 \approx 1$). The sum of the 2- and 3-jet cross sections is finite, since if the first order virtual corrections to the 2-jet cross section are taken into account (see Fig. 1b) the divergencies in the 3-jet cross section are canceled. This corresponds to the Kinoshita-Lee-Nauenberg theorem in QED[20], which guarantees that if one sums over all collinear and soft photons, the total cross section will be finite. Furthermore, the cross section stays finite for massless particles (no mass singularities).

Eq. 9 gives the cross section for bare partons. In order to calculate an observable cross section one has to take into account the finite jet resolution, which implies that one observes only jets 'dressed' by the accompanying soft gluons. The situation is similar to QED: the observed cross section $\sigma(e^+e^- \to \mu^+\mu^-)$ contains also that part from the radiative cross section $\sigma(e^+e^- \to \mu^+\mu^-\gamma)$ for which the photon is either too soft or too collinear to be detected. Correspondingly, the observable 2-jet cross section contains that part of the 3-jet cross section for which the gluon jet is irresolvable from the quark jets (dressed jets).

Two criteria have been used to define the jet resolvability:

- ϵ, δ cuts. In this case two partons are considered to be irresolvable if either one or both partons are too soft, i.e. have a parton energy less than $\epsilon\sqrt{s}/2$ or the partons are collinear, i.e. the angle between the partons is less than δ.
- y-cuts. In this case 2 partons are considered to be irresolvable if their scaled invariant mass is below a certain minimum: $(p_i+p_j)^2/s \leq y_{min}$. It should be noted that y cuts are Lorentz invariant, while the ϵ, δ cuts are not, so the ϵ, δ cuts refer to the centre of mass system.

2.3 Second order QCD predictions

In second order QCD one has to take into account the production of 4-jets, as shown by the graphs in Fig. 4 and the virtual corrections to the 3-jet cross section as shown in Fig. 2b. Again, the observable jet cross sections have to include the contributions from higher order graphs with irresolvable partons, so schematically one gets in second order QCD:

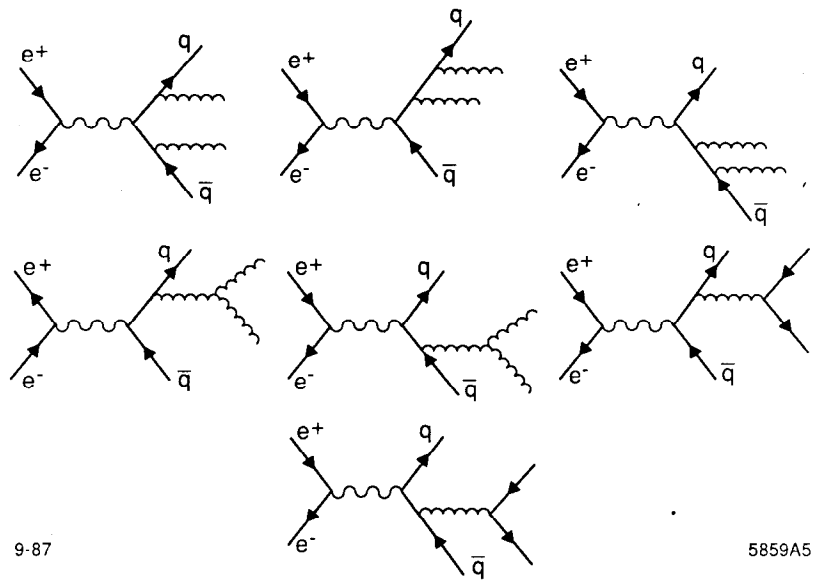

Fig. 4: Leading order Feynman diagrams for the production of 4-jet events in e^+e^- annihilation.

$$\sigma^{obs}_{2-jet} = \sigma^{tree}_{2-jet} + \sigma^{virt}_{2-jet}\left[O(\alpha_s)\right] + \sigma^{virt}_{2-jet}\left[O(\alpha_s{}^2)\right] + \sigma_{3-soft} + \sigma_{4-soft} \tag{10}$$

$$\sigma^{obs}_{3-jet} = \sigma^{tree}_{3-jet} + \sigma^{virt}_{3-jet}\left[O(\alpha_s{}^2)\right] + \sigma'_{4-soft} \tag{11}$$

$$\sigma^{obs}_{4-jet} = \sigma^{tree}_{4-jet} \tag{12}$$

In these equations σ_{3-soft} and σ_{4-soft} are the 3- and 4 jet cross sections with irresolvable partons, which have to be integrated over the corresponding region of phase space and then added to the 2- or 3-jet cross section. These definitions are exemplified in Fig. 5 for the 3-jet case: σ_{3-soft} is the 3-jet cross section integrated over the shaded area with $y_{ij} \leq y_{min}$, while σ^{tree}_{3-jet} is the cross section integrated over the remaining part of phase space. As can be seen from Eqs. 10 to 12 the 2-jet cross section is the most elaborate one to calculate, but in actual Monte Carlos the 2-jet cross section is defined as the difference between the total cross section and the dressed 3- and 4-jet cross sections, which all have been calculated. Also the 2-jet cross section was calculated recently, which allows a check of the consistency of the calculations[21].

The 4-jet cross sections in second order has only contributions at the tree level(see Eq. 12), which have been calculated by various groups and all agree[22]. However, the 3-jet cross sections in second order requires virtual corrections (see Eq. 11 and Fig. 2b), which were calculated by several groups (denoted by the first letters of the author names): GKS[23], ERT[24], and VGO[25]. Originally the conclusions were rather different: The last 2 groups claimed the second order virtual corrections to be large, while the first group claimed these corrections to be small. It is now understood that these different conclusions came from the different jet-resolution criteria[26]: The first group included jet resolution ('dressed jets'),

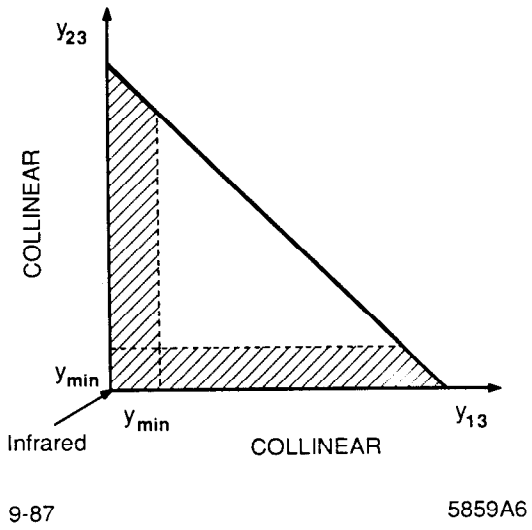

Fig. 5: $q\bar{q}g$ phase space. The shaded area with $y_{ij} \leq y_{min}$ is counted as part of the 2-jet cross section .

while the other groups calculated the cross section for bare partons. In the latter case the 4-jet cross section dominates and the 3-jet cross section becomes negative. An example of these cross sections as function of the jet resolution is shown in Fig. 6[27]. As can be seen, for small y-cuts (i.e. 1/y large) large cancelations occur corresponding to large second order corrections.

Insisting on a positive 3-jet cross section requires the y-cut to be above ≈ 0.01 (depending on α_s). On the other hand one should not take too large y-cuts, since in this case most of the 3-jet events are recombined to 2 jets. Reasonable cuts are in the range 0.01 to 0.05, although some experimental distributions prefer values closer to 0.01.

The GKS matrix element has been implemented in the LUND Monte Carlo and the ERT matrix element has been made suitable for Monte Carlo generators by Zhu[28] from the MARK-J Collaboration by complementing it with a jet dressing scheme along the lines of Ali[29] and Kunzst[30]. It was implemented in the LUND Monte Carlo by Csikor[31].

For the actual Monte Carlo implementations the GKS matrix element gives a lower 3-jet cross section than the ERT matrix element as shown in Fig. 7: at y=0.02(0.04) ERT gives a factor 2.5 (1.5) larger second order contribution, which corresponds to a 12(7) % increase in the total 3-jet rate for α_s=0.15. Possible causes for the differences are the approximations made in the GKS calculations and the ambiguity concerning the treatment of soft gluons in 4-jet events:

- In the ERT implementation the irresolvable partons are recombined with the nearest parton either by summing the 3-momenta or 4-momenta (momentum and energy schemes, respectively). The nearest parton is the one which yields the smallest invariant mass. The difference between the energy- and

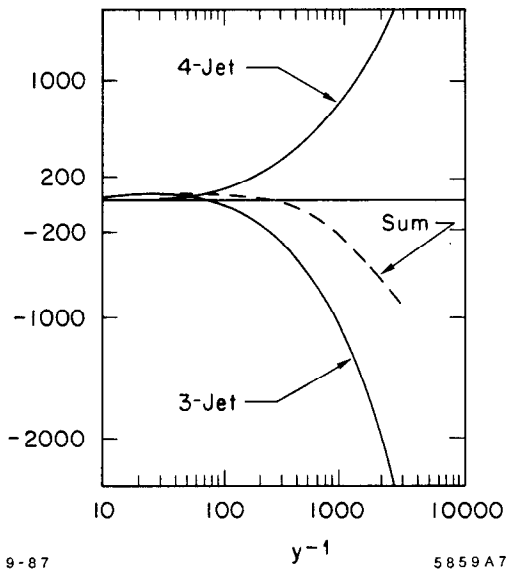

Fig. 6: The 3- and 4-jet cross section as function of the jet resolution parameter 1/y.

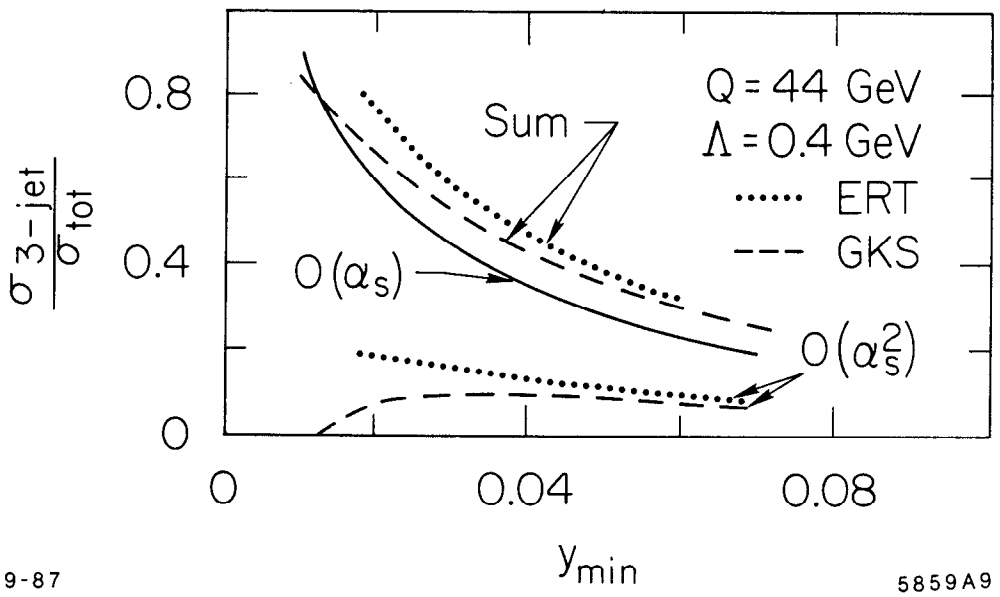

Fig. 7: The 3-jet cross sections as function of the y-cut for the ERT- and GKS matrix elements .

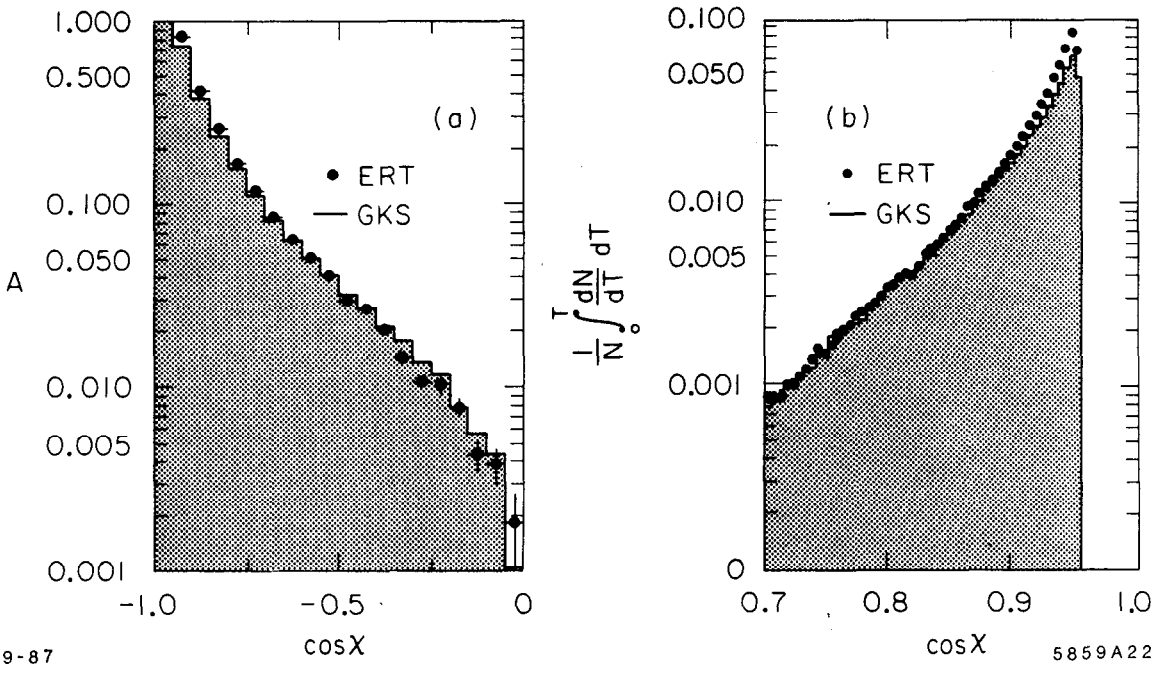

Fig. 8: Integrated thrust (a) and integral of the AEEC (b) for the 2 different matrix elements ERT(solid dots) and GKS(histogram). Both distributions are plotted at the parton level for $\sqrt{s}$=44 GeV, $\Lambda_{\overline{MS}}$=400 MeV and y_{min}=0.02.

momentum scheme is small [28].

- In the GKS implementation with y-cuts the recombination scheme is similar to the previous one. However, if ϵ, δ cuts are used, the partons failing the δ cuts are recombined, but the partons failing the ϵ cuts are discarded and the energy of the remaining partons is rescaled, so here the energy of the soft partons is distributed over all partons, while in the previous scheme it was added to the nearest parton.

The difference between the various recombination schemes has been studied in detail[28,32]. Unfortunately, no clear-cut theoretical argument can be given for either of the dressing schemes, but the differences concern mainly soft gluons. So if one studies gluons only in the perturbative regime, the differences between the matrix elements are small, especially if one uses y-cuts (implying similar dressing schemes). This is demonstrated in Fig. 8 for the integrated parton thrust for dressed 3-jet events and the asymmetry in energy weighted angular correlations (AEEC, see Sect. 5.3). Low thrust values and large angles correspond to regions where the hard gluons dominate. For thrust values integrated up to 0.9 the difference is negligible. For larger values ERT is ≈25% higher. For the AEEC the difference depends on the angular range considered: for $\cos\chi > -0.7$ the GKS prediction is somewhat above ERT while for the small angle region ERT is higher. A fit of the QCD calculation in the range $\cos\chi > -0.7$ yields less than 30 MeV difference in the QCD scale parameter between the two matrix elements.

TASSO [33] studied the differences between the matrix elements using ϵ, δ cuts (implying different dressing schemes). They find from the AEEC a difference in α_s of $\approx$15% even after correcting for some of the missing diagrams in the implementation of the GKS matrix element.

MARK-II[34] studied the difference between GKS and a new matrix element by Gottschalk and Shatz, which is also based on analytic formulae[26], but it does not use the approximations made by GKS. They find a 10% lower value of α_s with this new matrix element, if they fit the AEEC for $\cos\chi > -0.88$.

So it is important in the comparison of results to keep in mind which matrix element was used and which variable was fitted in what range.

2.4 Definition of the running coupling constant

The coupling constant is not constant, but varies with Q^2 both in QED and in QCD. However, in QED the coupling constant increases as function of Q^2, while in QCD the coupling constant decreases. A simple picture for this behaviour is the following:

- In QED the coupling constant decreases with increasing energy, since the photons which make up the electric field around an electric charge can be transformed into e^+e^- pairs. These e^+e^- pairs are oriented in the electric field (=polarized) and provide an effective shielding of the 'bare' electric charge. If the electric charge is probed at higher energies (or shorter distances), one penetrates the shielding from the vacuum polarization deeper and observes more of the bare charge, or equivalently one observes a larger coupling constant.

- In QCD the situation is more complicated: the colour charge is surrounded by a cloud of gluons and virtual $q\bar{q}$ pairs, but since the gluons themselves carry a colour charge, one has two contributions: a shielding of the bare charge by the $q\bar{q}$ pairs and an increase of the colour charge by the gluon cloud. The net effect of the vacuum polarization is an increase of the total colour charge, provided not too many $q\bar{q}$ pairs contribute (number of generations < 16, see hereafter). If one probes this charge at smaller distances, one penetrates part of the 'antishielding', thus observing a smaller colour charge at higher energies. So it is the fact that gluons carry colour themselves which make the coupling decrease at small distances (or high energies).

The effect of the virtual pairs surrounding an electric charge or colour charge can be calculated from the diagrams in Fig. 9. These diagrams are divergent for large Q^2. A theory is renormalizable if one can absorb all divergencies in the bare coupling constants. The first step in such calculations is the regularization of the divergencies, which is usually done with the dimensional regularization scheme of 't Hooft and Veltman[35]. In $n = 4 - 2\epsilon$ dimensions the bare coupling constant has the dimension of a mass. In order to make it dimensionless, one introduces an arbitrary parameter μ with the dimension of a mass and defines

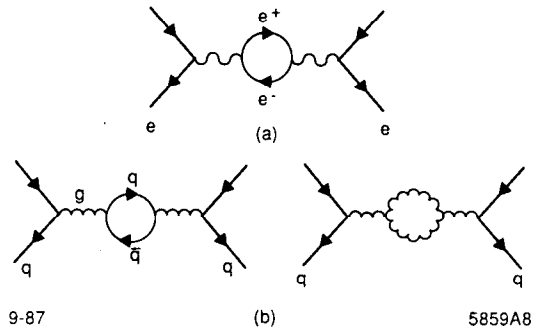

Fig. 9: The lowest order vacuum polarization diagrams leading to a renormalized electric - (a) and colour charge (b).

the coupling as $g(\mu^2) = \mu^\epsilon g$ and $\alpha_s = g^2/4\pi = \alpha_s(\mu^2)$ The diagram in Fig. 9a contributes a term $\approx \frac{\alpha(\mu^2)}{3\pi} ln\frac{Q^2}{\mu^2}$ to the cross section, if $Q^2 >> \mu^2$. In QED it is customary to choose for μ the electron mass m_e. In this case one can absorb the divergent vacuum polarization in an effective coupling constant by modifying the fine structure constant $\alpha = e^2/4\pi$ as follows:

$$\alpha(Q^2) = \alpha(1 + \frac{\alpha}{3\pi} ln\frac{Q^2}{m_e^2}) \tag{13}$$

If one sums more loops, this yields terms $(\frac{\alpha}{3\pi})^n (ln\frac{Q^2}{m_e^2})^m$ and retaining only the leading logarithms (i.e. n=m), the addition of these terms yields:

$$\alpha(Q^2) = \frac{\alpha}{(1 - \frac{\alpha}{3\pi} ln\frac{Q^2}{m_e^2})} \tag{14}$$

since

$$\sum_{n=0}^{\infty} x^n = \frac{1}{1-x}. \tag{15}$$

Of course, the total Q^2 dependence is obtained by summing over all possible fermion loops in the photon propagator.

The diagrams of Fig. 9b yield similarly:

$$\alpha_s(Q^2) = \alpha_s(\mu^2) \left[1 - \frac{\alpha_s(\mu^2)}{4\pi} \left(11 - \frac{2N_f}{3}\right) ln\frac{Q^2}{\mu^2}\right] \tag{16}$$

Note that α_s decreases with increasing Q^2 if $11 - 2N_f/3 > 0$ or $N_f < 16$, thus leading to asymptotic freedom at high energy. This is in contrast to the Q^2 dependence of $\alpha(Q^2)$ in Eq. 13, which increases with increasing Q^2. Since α_s becomes infinite at small Q^2, one cannot take this scale as a reference scale, as was done in the case of QED.

A physical quantity should not depend on the spurious parameter μ, at least if one calculates it to all orders. If one calculates only up to a finite order, one can minimize the higher order terms by a suitable choice of μ. In lowest order μ is arbitrary, but in higher orders the loop calculations contain terms $ln\frac{Q^2}{\mu^2}$ and to keep these terms small, it is best to choose μ^2 to be of the same order as Q^2, where Q^2 is the relevant physical scale of the process.

The higher order corrections are usually calculated with the renormalization group technique, which yields for the μ dependence of α_s :

$$\mu\frac{\partial\alpha_s}{\partial\mu} = \beta_0{\alpha_s}^2 + \beta_1{\alpha_s}^3 + \beta_2{\alpha_s}^4 + ... \tag{17}$$

The first two terms in this perturbative expansion are renormalization-scheme independent and given by:

$$\beta_0 = -\frac{1}{2\pi}\left[11 - \frac{2N_f}{3}\right] \tag{18}$$

$$\beta_1 = -\frac{1}{4\pi^2}\left[51 - \frac{19N_f}{3}\right] \tag{19}$$

Higher order terms depend on the renormalization prescription. In the $\overline{MS}$ scheme β_2 has been calculated [36]:

$$\beta_2 = -\frac{1}{64\pi^3}\left[2857 - \frac{5033N_f}{9} + \frac{325N_f^2}{27}\right] \tag{20}$$

Eq. 17 can be integrated as follows (retaining only the first two terms):

$$\int_{\mu_0}^{\mu}\frac{d\mu}{\mu} = \int_{\alpha_s(\mu_0)}^{\alpha_s(\mu)}\frac{d\alpha_s}{{\alpha_s}^2(\beta_0 + \beta_1\alpha_s)} \tag{21}$$

Here μ_0 is a reference mass scale. Instead of introducing two separate lower bounds in the integrals in Eq. 21, one usually combines them by choosing for μ_0 the QCD scale Λ, which fulfills the boundary condition $\alpha_s(\mu_0 = \Lambda) = \infty$. In this case the solution of Eq. 21 is:

$$\frac{1}{\alpha_s(\mu^2)} = -\frac{\beta_0}{2}ln\frac{\mu^2}{\Lambda^2} + \frac{\beta_1}{\beta_0}ln(1 + \frac{\beta_0}{\beta_1\alpha_s(\mu^2)}) \tag{22}$$

The last term in this equation can be approximated by $ln(1/\alpha_s) \approx ln(ln\frac{\mu^2}{\Lambda^2})$, if $\mu^2 >> \Lambda^2$. One can then write a functional form for α_s:

$$\frac{1}{\alpha_s(\mu^2)} = -\frac{\beta_0}{2}ln\frac{\mu^2}{\Lambda^2} + \frac{\beta_1}{\beta_0}ln(ln\frac{\mu^2}{\Lambda^2}) \tag{23}$$

which is approximated in the Particle Data Book [37] as (using $\mu = Q$):

$$\alpha_s(Q^2) = \frac{12\pi}{(33 - 2N_f)ln\frac{Q^2}{\Lambda^2}}\left[1 - 6\frac{153 - 19N_f}{(33 - 2N_f)^2}\frac{ln(ln\frac{Q^2}{\Lambda^2})}{ln\frac{Q^2}{\Lambda^2}}\right] \tag{24}$$

The approximations in Eqs. 23 and 24 both introduce an error of $\approx$ **15%** in Λ for a given α_s, but they are of opposite sign and largely cancel each other, *so we will use Eq. 24 hereafter.*

In the $\overline{MS}$ scheme N_f is the number of flavours with mass $m_q < \mu$ (not $2m_q < \mu$). If μ becomes larger than m_q at a certain energy, one has to increase N_f. With the previous definition of α_s, this would give a discontinuity in α_s, since α_s depends explicitly on N_f. Such a discontinuity is unphysical, since only the running of the coupling constant can change if more quarks contribute to the vacuum polarization, not its value. This can be remedied in the previous formula either by the use of a different Λ for each number of flavours (as is usually done) or one has to incorporate explicitly a counter term in the definition of α_s. E.g. if Λ_5 is defined for 5 flavours, then for $m_c < Q < m_b$ Eq. 24 becomes[38]:

$$\alpha_s(Q^2) = \frac{12\pi}{(33-2N_f)ln\frac{Q^2}{\Lambda^2}}\left[1 - \frac{\frac{462}{625}ln(ln\frac{Q^2}{\Lambda^2}) - \frac{2}{25}\left(ln\frac{m_b^2}{\Lambda_5^2} + \frac{963}{575}ln(ln\frac{m_b^2}{\Lambda_5^2})\right)}{ln\frac{Q^2}{\Lambda^2}}\right] \quad (25)$$

Alternatively, one can neglect the last term in the brackets and use for $m_c < Q < m_b$ a different Λ_4 defined by[38]:

$$\frac{\Lambda_4}{\Lambda_5} \approx \left[\frac{m_b^2}{\Lambda_5^2}\right]^{\frac{1}{25}}\left[ln\frac{m_b^2}{\Lambda_5^2}\right]^{\frac{963}{14375}} \quad (26)$$

This ratio varies from 1.57 to 1.47(1.41) for Λ_5 varying from 100 to 200(300) MeV.

In summary one can absorb the divergent vacuum polarization diagrams in the coupling constant, which then becomes dependent on Q^2. Instead of quoting a coupling constant at a given Q^2, one can use the scale parameter Λ, which is independent of Q^2 and can be defined by the boundary condition requiring $\alpha_s(\mu = \Lambda) = \infty$.

2.5 The total hadronic cross section

The normalized total cross section for multihadron production from e^+e^- annihilation is defined as the ratio R

$$R \equiv \frac{\sigma[e^+e^- \to \gamma, Z^0 \to hadrons]}{\sigma[e^+e^- \to \gamma \to \mu^+\mu^-]} \quad (27)$$

where the numerator is the hadron production cross section corrected for QED radiative corrections. The denominator is just a calculated quantity equal to the pointlike QED cross section: $4\pi\alpha^2/3s$.

At the highest PETRA energies Z^0 exchange and, to a lesser extent, the interference between the photon and Z^0 exchange becomes important. The prediction of the Standard Model can be written as:

$$R = R_0\left[1 + \frac{\alpha_s(s)}{\pi} + C_2\left(\frac{\alpha_s(s)}{\pi}\right)^2\right] \quad (28)$$

with (see Eq. 3)

$$R_0 = 3\sum_q \left[e_e^2 e_q^2 + 2e_e e_q v_e v_q \Re(\chi) + (v_e^2 + a_e^2)(v_q^2 + a_q^2)|\chi|^2\right] \tag{29}$$

Here we have neglected quark mass effects. At the lowest PETRA energies (14 GeV) the effect of m_b is 1%, which has been taken into account in the fits described hereafter[39]. The constant C_2 depends on the renormalization scheme chosen to minimize the higher order corrections. In the $\overline{MS}$ scheme it is given by[40]:

$$C_2 = 1.986 - 0.115 N_f \tag{30}$$

provided the scale μ of α_s is taken to be $\sqrt{s}$. If another renormalization point is chosen, e.g. $\mu = x\sqrt{s}$, one obtains a different R, α_s, and C_2[41,42,43,44]:

$$R' = R + O({\alpha_s}^3) \tag{31}$$

$${\alpha_s}' = \alpha_s + \frac{\beta_0}{\mu}{\alpha_s}^2 d\mu + O({\alpha_s}^3) \tag{32}$$

$$C_2' = C_2 + \frac{\partial C_2}{\partial \mu} d\mu \tag{33}$$

Eq. 33 is just by definition and Eq. 32 follows from Eq. 17. If one neglects terms of $O({\alpha_s}^3)$ one obtains by simply equating $R' = R$:

$$\frac{\partial C_2}{\partial \mu} + \frac{\pi\beta_0}{\mu} = 0 \tag{34}$$

or

$$C_2' = C_2 - \pi\beta_0 ln x \tag{35}$$

and

$$R = R_0\left[1 + \frac{\alpha_s(x^2 s)}{\pi} + C_2'\left(\frac{\alpha_s(x^2 s)}{\pi}\right)^2\right] \tag{36}$$

This last expression differs from Eq. 28 only by the constant C_2 and the renormalization point, so one sees that changing the renormalization point is equivalent to changing renormalization schemes (implying different coefficients C_2).

2.6 Choice of renormalization scheme

Physical quantities do not depend on the renormalization scheme (RS) or renormalization point (μ in Sect. 2.3), if they are calculated to all orders in perturbation theory. However, if one calculates only up to order n, thus neglecting terms of $O(n+1)$, then different RS's can also differ by terms of $O(n+1)$. Stevensen[42] proposed to choose for each process a renormalization point such that the observable shows minimal sensitivity to the RS, i.e. $\partial\Re/\partial(RS)$=0 or $\partial\Re/\partial ln\mu$=0.

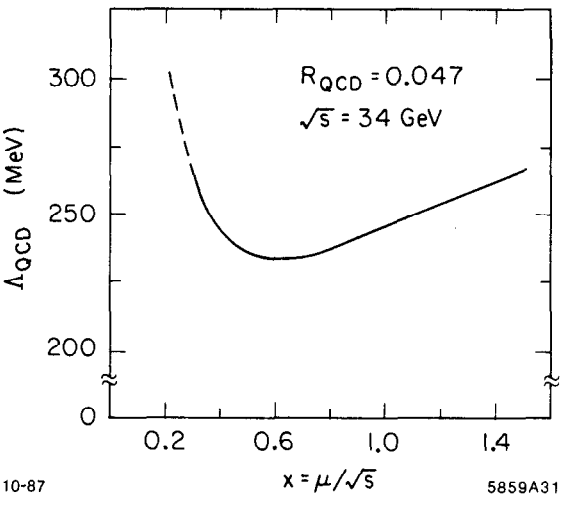

Fig. 10: The dependence of the QCD scale Λ on the renormalization point μ (normalized to $\sqrt{s} = 34$ GeV) given a QCD contribution to R of 0.047. The curve was obtained by choosing x, then calculating the value of α_s for a given R from Eqs. 35 and 36, and then determining Λ from Eq. 22. Note that one cannot choose x below ≈0.20, since in that case the second order contribution becomes so large and negative that no positive solution for the QCD contribution to R can be found.

This 'principle of minimal sensitivity' (PMS) can be easily applied to the measurement of R and we will then compare it to other renormalization schemes or prescriptions to choose a certain scale μ.

For a given value of R one can study the dependence on μ with Eqs. 35 and 36 and one can determine the resulting variation of α_s as function of $x = \mu/\sqrt{s}$ or more easily Λ as function of x, since Λ is independent of μ. Fig. 10 shows this dependence. The PMS value of x is obtained by requiring

$$\frac{\partial R}{\partial ln\mu} = \frac{\partial R}{\partial \alpha_s}\frac{\partial \alpha_s}{\partial ln\mu} + \frac{\partial R}{\partial C_2'}\frac{\partial C_2'}{\partial ln\mu} = 0 \tag{37}$$

The partial derivatives are easily calculated from Eqs. 17, 35 and 36 and inserting them into Eq. 37 yields:

$$\left(\frac{1}{\pi} + 2\frac{\alpha_s}{\pi^2}C_2'\right)\alpha_s{}^2\left(\beta_0 + \beta_1\alpha_s\right) - \beta_0\frac{\alpha_s{}^2}{\pi} = 0 \tag{38}$$

or for $C_2' = C_2^{opt}$ corresponding to the PMS criterion

$$C_2^{opt} = -\frac{\pi\beta_1}{2\beta_0\left[1 + \frac{\beta_1}{\beta_0}\alpha_s\right]} \approx -\frac{\pi\beta_1}{2\beta_0} \tag{39}$$

This corresponds to an optimum scale μ^{opt} given by $x^{opt} = \mu^{opt}/\sqrt{s}$ (from Eq. 35):

$$ln\ x^{opt} \approx \frac{1.41}{\pi\beta_0} + \frac{\beta_1}{2\beta_0^2}. \tag{40}$$

The value of $x^{opt} \approx 0.59$ for five flavours corresponds to the minimum of the curve in Fig. 10, since for this line R is constant, so Eq. 37 is automatically satisfied if $\partial\Lambda/\partial\mu$=0[43].

Other renormalization schemes absorb different factors in the coupling constant, yielding different values of Λ; they are related to each other by a one-loop calculation as was first pointed out by Celmaster and Gonsalves[45].

However, the ratio μ/Λ is similar in each RS[42][2], so instead of varying Λ one can study the RS dependence by studying the μ dependence as mentioned also in the previous section. E.g. one of the MOM (Momentum Subtraction) schemes yields[41]: $C_2 = -2.193 + 0.162N_f$. The same value can be obtained in the $\overline{MS}$ scheme for $x = 0.48$ (using Eq. 35).

The RS schemes $\overline{MS}$ and MOM define the renormalization group equation (Eq. 17), but they do not specify the scale μ, so they have to be complemented by additional criteria to choose the scale (upper limit of integration in Eq. 21). Here one usually chooses a large scale typical for the reaction, e.g. $\mu = \sqrt{s}$ in case of R or one uses the PMS criterion, but other criteria can be used too.

For example, the FAC (Fastest Apparent Convergence) requires the second order corrections to vanish, which corresponds to $x = 0.69$. Brodsky, Lepage and Mackenzie (BLM)[46] choose the scale, which absorbs all vacuum polarization contributions into the coupling, which yields $C_2' = 0.08$ independent of N_f. In the $\overline{MS}$ scheme this value of C_2' corresponds to $x = 0.71$

So one sees that typical choices of RS's or scales correspond to x between 0.5 and 1.0. Λ varies less than 5% for this range of x (see Fig. 10), so the uncertainty from the renormalization scheme dependence is of this order of magnitude.

2.7 How to compare the Standard Model with data?

Not well determined in the SM are:

- the Higgs sector
- the strong coupling constant
- the weak properties of heavy quarks

In e^+e^- annihilation one gets a handle on the last two points, since

- The strong coupling constant can be either determined from the increase in the total hadronic cross section due to gluon bremsstrahlung or from the determination of the number of 3-jet events. The first one has the advantage, that it is theoretically very clean, but the effect is not large, ($\approx$ 5 % increase in R at 34 GeV), so the experimental errors dominate. In the case of the multijet analysis uncertainties from uncalculable fragmentation effects dominate the error.

[2]The optimum value of μ/Λ is an RS invariant.

- Above threshold one can study both heavy and light quarks in contrast to e.g. deep inelastic lepton nucleon scattering, where only the electroweak properties of light quarks can be studied.

Several strategies can be followed in the analysis:

- Determine the vector and axial vector coupling constants of the individual quarks separately. The axial coupling constants can be determined from the asymmetry, which contains the product $a_e a_q$ (see Eq. 8). The asymmetry can be determined for a specific quark flavour by a suitable flavour tagging technique (high p_t leptons or heavy meson identification) or averaged over all quarks. All asymmetry measurements sofar have been found to be in agreement with the Standard Model, although the errors are large[47]. Therefore we will accept in the following the basic assumption that all matter fields belong to weak isospin doublets, which then fixes uniquely the axial vector couplings of all leptons and quarks, since it is given by the position in the doublet ($a = I_3^L - I_3^R$).

- With the axial vector couplings of quarks and leptons fixed, one can proceed to determine the vector couplings from the total hadronic cross section. These depend on the single parameter $\sin^2\theta_W$, once the weak isospin structure has been fixed (see Eq. 5). The consistency of the vector couplings with the Standard Model can be checked by comparing the fitted $\sin^2\theta_W$ value with the world average.

The Higgs bosons are difficult to search for, since the mass is unknown and the production cross sections are small. The ρ parameter can deviate from 1 in case of a more complicated Higgs sector. From an analysis of data on neutral current interactions ρ is constrained to 0.998 ± 0.009[48]. Therefore we will assume the standard Higgs structure with $\rho = 1$ in what follows.

3 Jet Physics

Since free quarks have not been observed, QCD has to be complemented by the hypothesis that physical states are colour singlets, so if energetic quarks are produced, they are converted into hadrons by the strong forces. This hadronization can be described by simple phenomenological models, in which the hadrons are created with limited transverse momenta. This automatically leads to jet production at high energies: since the multiplicity is only rising slowly with energy ($n_{ch} \propto lns$) the jets become more and more collimated. The cone angle of the jet will decrease roughly as:

$$\delta \approx \frac{< p_\perp >}{< p_{||} >} \approx \frac{< p_\perp >}{s/ < n_{ch} >} \propto \frac{lns}{s} \tag{41}$$

Therefore only at high energies will one be able to resolve the jets in multijet events. When PETRA started operating around 30 GeV, 2-jet events were very

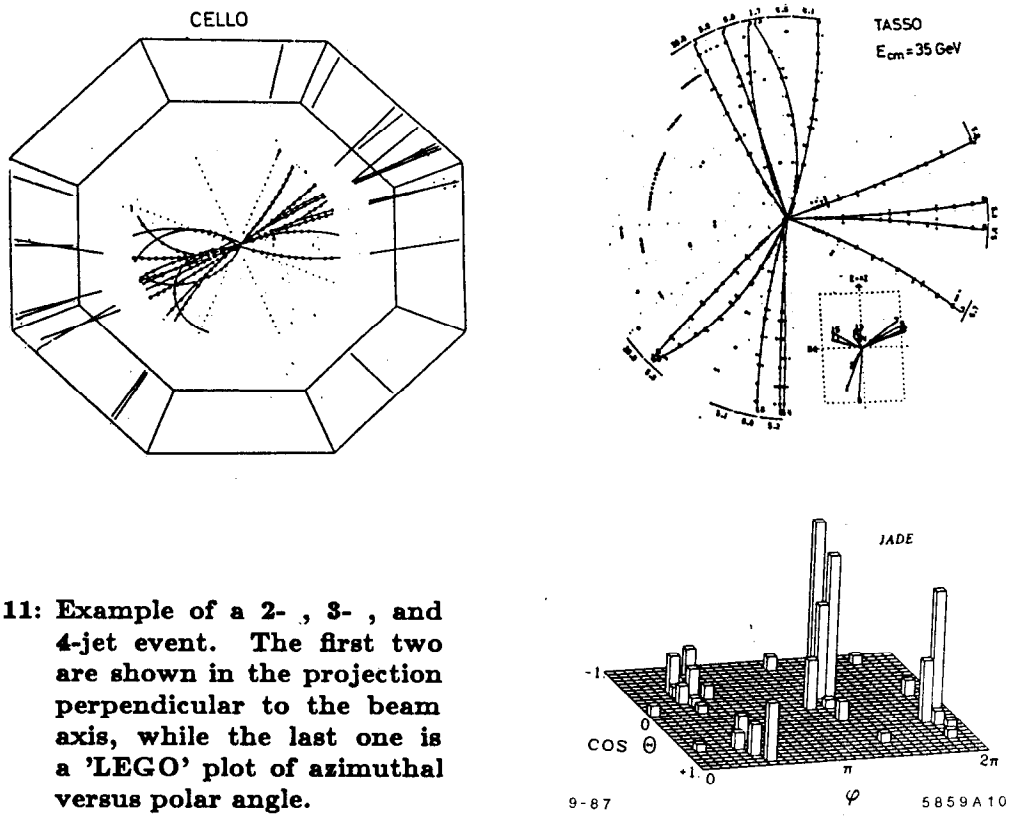

Fig. 11: Example of a 2- , 3- , and 4-jet event. The first two are shown in the projection perpendicular to the beam axis, while the last one is a 'LEGO' plot of azimuthal versus polar angle.

obvious just by visually scanning the events, so one did not need statistical methods. Furthermore, a sizeable fraction of events showed a clean 3-jet structure and sometimes 4-jets were observed. Fig. 11 shows some examples.

Several methods have been used to classify multijet events, e.g. cluster algorithms yielding directly the number of jets, the sphericity, aplanarity, thrust, oblateness, spherocity, triplicity and others. Most of them have been incorporated as utility routines in the LUND Monte Carlo, so the interested reader can consult the descriptions there[49]. Detailed studies showed that:

- From the angular distribution of two jet events it is clear that the original partons have spin 1/2, as shown in Fig. 12 by the characteristic $1 + a\cos^2\theta$ distribution of the sphericity axis: the best fit yields $a = 1.01 \pm 0.1$, which is close to the expected value of $a = 1$ for spin 1/2 quarks and far from the value of $a = -1$ for spin 0 quarks.

- The 3-jet events are planar and originated from a bremsstrahlung spectrum. Two typical plots are shown in Figs. 13 and 14. The first one shows that the broadening of the transverse momentum in a jet takes place mainly in the event plane, while $< p_t^{out} >$ hardly changes as function of energy, thus excluding the possibility that the p_t broadening is caused by an energy dependent fragmentation effect. The second plot shows that the oblateness is only well described by the Monte Carlo if gluon radiation is included.

- The angular distributions of the jets relative to each other in 3-jet events depend on the spin of the gluon. A simple distribution was proposed by Ellis

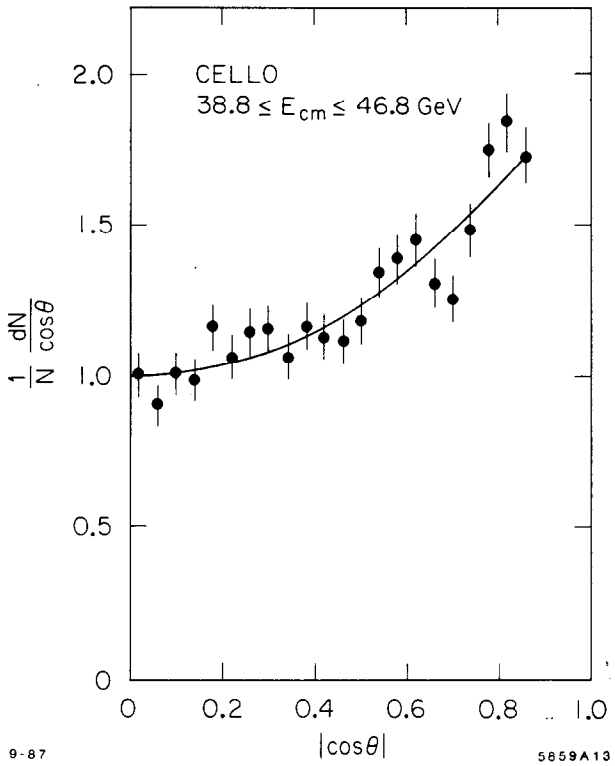

Fig. 12: The angular distribution of the sphericity axis of multihadronic events. The curve is the fitted $1 + a\cos^2\theta$ distribution with $a = 1.01 \pm 0.1$.

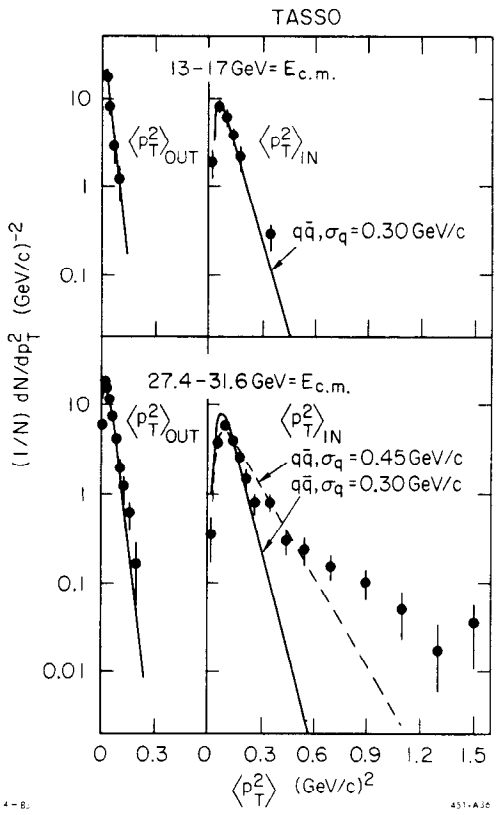

Fig. 13: The transverse momenta in a jet as function of centre of mass energy. The data at lower energies (top) can be described by $q\bar{q}$-production while the events at high energies develop a planar event structure, as expected for $q\bar{q}g$ production. Note that the transverse momentum distribution perpendicular to the event plane, shown on the left-hand side, is found to be similar for both energies.

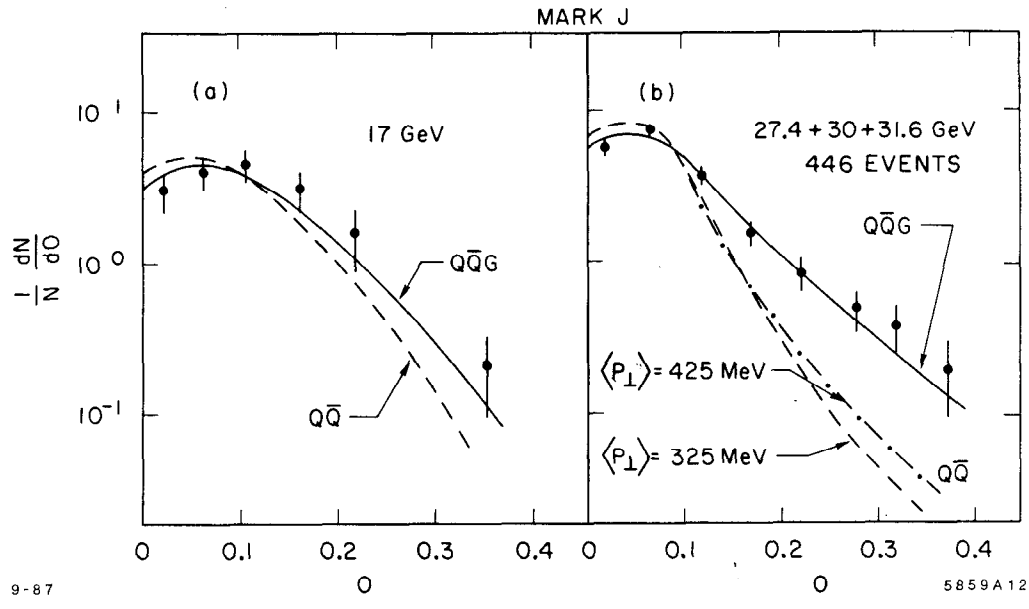

Fig. 14: The oblateness compared with a Monte Carlo simulation with and without gluon radiation.

and Karliner[50]: in the rest frame of the hardest jet the angle between the remaining jets is given by:

$$\cos\tilde{\theta} = \frac{x_2 - x_3}{x_1} = \frac{sin\theta_2 - sin\theta_3}{sin\theta_1} \tag{42}$$

The relation between the angles and fractional energies is given by energy momentum conservation for massless partons:

$$x_i = \frac{sin\theta_i}{sin\theta_1 + sin\theta_2 + sin\theta_3}. \tag{43}$$

Here θ_i is the angle between the 2 jets opposite to jet i. The scalar theory does not fit the data as shown by TASSO[51] (see Fig. 15).

Another simple way to test the gluon spin is the determination of the energy of the most energetic cluster in 3-jet events, which is simply x_1 for three partons. For a vector gluon x_1 is determined by the differential distributions given in Eq. 9. For a scalar gluon it is[27]:

$$\frac{d^2\sigma}{\sigma^{(2)}dx_1dx_2}(e^+e^- \to q\bar{q}g) = \frac{\widetilde{\alpha}_s}{2\pi}C_F\frac{x_3^2}{(1-x_1)(1-x_2)} + 1,2,3\ cyclic\ perm. \tag{44}$$

Here $\widetilde{\alpha}_s$ is the coupling constant for the scalar theory. This distribution has been checked by many experiments[52] and they all find much better agreement for a spin-1 gluon as shown in Fig. 16.

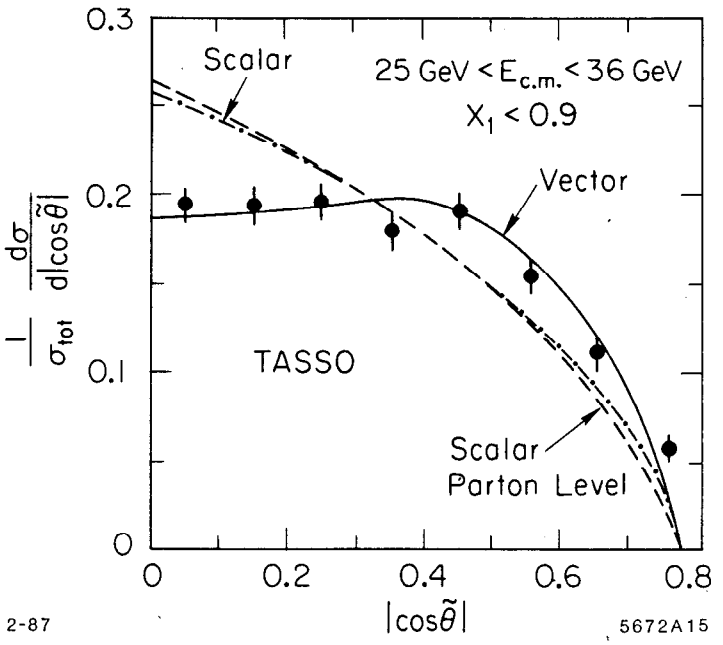

Fig. 15: The observed distribution of the Ellis-Karliner variable for events in the 3-jet region defined by $x_1 < 0.9$. The full curve shows the prediction to $O(\alpha_s)$ for vector gluons, the dashed curves the predictions for scalar gluons at the parton and hadron level. These almost coincide, thus showing that fragmentation effects are not important for the shape of these curves.

4 How to compare Jets with Partons ?

One of the basic difficulties with testing QCD quantitatively is the fact that QCD deals with calculations at the parton level, while experiments observe hadrons. The transition from partons to hadrons cannot be calculated at present, since this belongs to the 'non-perturbative' region of QCD. Therefore one has to use phenomenological models to describe the transition from partons to hadrons. This transition is usally called hadronization or fragmentation.

4.1 Fragmentation models

Several fragmentation models are on the market:

- Independent fragmentation models. In this case the original description of Field-Feynman[53] for single quarks is extended to each parton individually. The gluon is either treated as a quark (Hoyer et al.[54]) or split into two quarks according to the Altarelli-Parisi splitting functions (Ali et al.[55]). Due to the enforcement of energy-momentum conservation after the fragmentation of each parton, correlations between the outgoing jets are imposed, which depend on the rather arbitrary choice of the energy-momentum conservation mechanism, as will be discussed below.
- String fragmentation. In this case the hadrons are formed along a string stretched between the outgoing partons. The string tension represents the

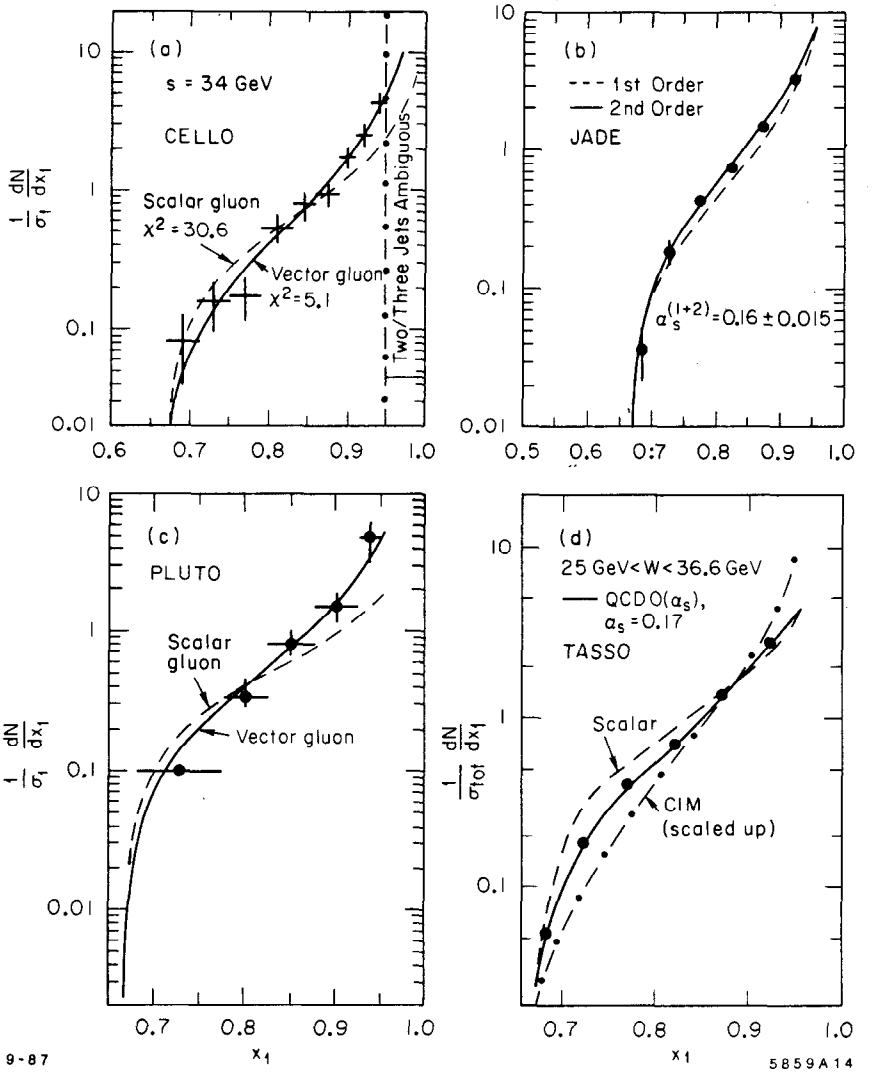

Fig. 16: The distribution of the fractional momentum of the highest energy jet in 3-jet events compared with various models. A vector gluon describes the data, while a scalar gluon does not. Also the second order QCD calculation fits better than the first order one (JADE) and the constituent interchange model (CIM) is excluded (TASSO).

strength of the colour field (growing linearly with distance) and as soon as the tension becomes large enough, the energy is converted into mass by the formation of $q\overline{q}$ pairs at the breakpoints of the string. Such a model introduces explicitly correlations between the outgoing partons, which are experimentally testable, as will be discussed later. The string fragmentation has been implemented in a widely used program written by T. Sjöstrand[49].

- Parton shower generation. In this case leading log calculations are used to generate events with many partons in the initial state in contrast to the previously mentioned Monte Carlos, which generate states with at most 4 partons ($O(\alpha_s{}^2)$). Because of the leading log approximation, the hard gluon production does not correspond to the exact QCD first or second order matrix element. Therefore one has to do a joining of the exact matrix element and the leading log approximation, but one has to be careful to avoid double counting. This joining of the first order QCD and leading log matrix elements has been implemented in the new Monte Carlo of the LUND group[49]. Furthermore, this version JETSET6.3 has the possibility to switch on and off interference effects between the initial partons, which were among the differences of earlier versions of shower Monte Carlos by Gottschalk[56] and Webber[57].

4.2 Can one distinguish between the models?

The main difference between independent fragmentation (IF) and string fragmentation (SF) is in the different treatment of the gluon. So a difference can only be observed in 3-jet and 4-jet events. The parameters used for the description of 2-jet events are the same: a fragmentation function to describe the longitudinal momentum spectra of the hadrons, the variance of the gaussian used to generate limited transverse momenta, the ratio of vector to pseudoscalar mesons, the amount of s- and c-quarks generated during fragmentation, amount of diquarks (yielding baryons), and others.

In the SF model the gluon is part of a string stretched between the quarks. If the gluon is soft, the main effect will be to give some transverse momentum to the string, but the event remains 2-jet like. If the gluon is hard and at a large angle, it will give a large p_t to the string and generate a 3-jet-like event. However, since the gluon is connected via a string to both quarks it will drag both string pieces in the direction of the gluon, thus depleting the particle density on the other side. (see Fig. 17).

This string effect was first observed by JADE and later confirmed by several other experiments[58]. It is shown in Fig. 18: After selecting the hardest jet in 3-jet events, the particle density with respect to this direction (0^0 in Fig. 18) is clearly higher in the region between the most energetic and least energetic jet as compared to the particle density in the region between the two most energetic jets. The least energetic jet has the highest probability to be the gluon jet. It is compared with several models: clearly the string fragmentation model describes the data, while the independent fragmentation model does not. However, some

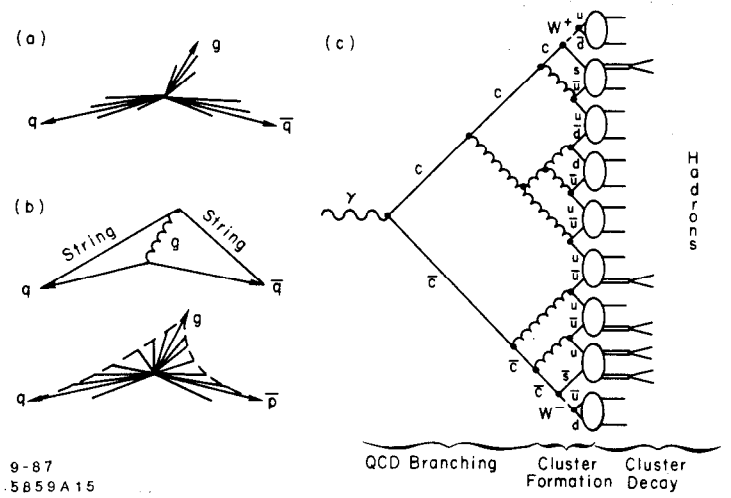

Fig. 17: Schematic picture of independent fragmentation(a) string fragmentation(b) and shower cascade Monte Carlo models(c).

parton shower models do reproduce the data too. Two effects contribute here:

- at the parton level a depletion of the $q\bar{q}$ region does occur if interference effects of multiple soft gluon emission are taken into account. This was first calculated by Azimov et al.[59] and proposed as an explanation why the fragmentation models based on the classical string picture describe the data.
- After generating partons, they are combined into clusters which then fragment into hadrons. If this is done via the string fragmentation model, it is hard to distinguish how much of the coherence effect is due to the interference and how much is due to the string fragmentation, since both introduce a coherence between the final state particles[60]. However, if one has no interference and no string fragmentation, so no coherence effects at all, the model cannot describe the data as shown by the curve from the Gottschalk Monte Carlo in Fig. 18b. Also in the Webber model the 'string' effect disappears, if the clusters are allowed to decay isotropically[61].

To test coherence effects in a model independent way, a nice experiment was proposed by Azimov et al.[59]. They consider the radiation from a $q\bar{q}$ pair, which can either radiate photons or gluons. In case of a gluon interference effects occur, while they are absent in case of a photon. So the coherence effects can be studied by comparing $q\bar{q}g$ events with $q\bar{q}\gamma$ events. This was first done by the TPC and MARK-II and recently by JADE[62]. Fig. 19 shows the ratio of the particle density in the $q\bar{q}$ region for $q\bar{q}g$ and $q\bar{q}\gamma$ events, where the $q\bar{q}$ region in the $q\bar{q}g$ events is defined as the region between the 2 most energetic jets. This ratio should be 1 if no coherence effects would be present, since the gluon and photon energies were chosen such that the kinematical configurations of both event types were similar.

One can argue that the IF fragmentation models can be discarded, since they do not describe the string effect. However, this affects only a small number of

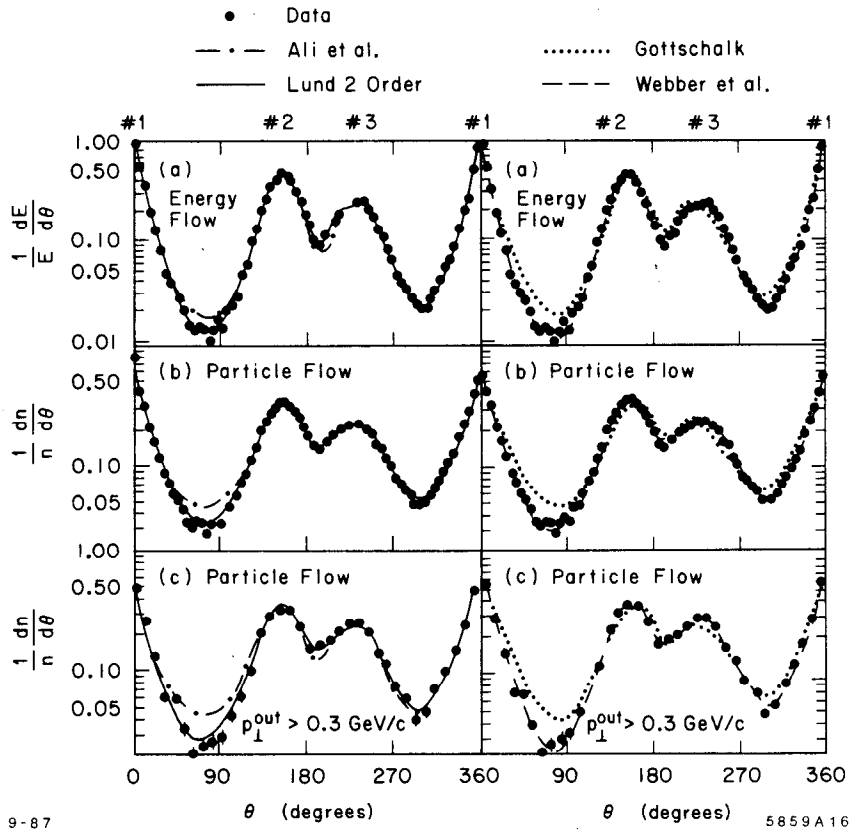

Fig. 18: The hadron flow in the plane of 3-jet events compared with different Monte Carlo models. Only the LUND and Webber Monte Carlos reproduce the depletion of particles between the two most energetic jets (around 70°). The effect is enhanced for particles with a large momentum out of the plane (see (c)), as expected if the effect occurs through a boost for which the relevant quantity is $m^2 + p_t^2$.

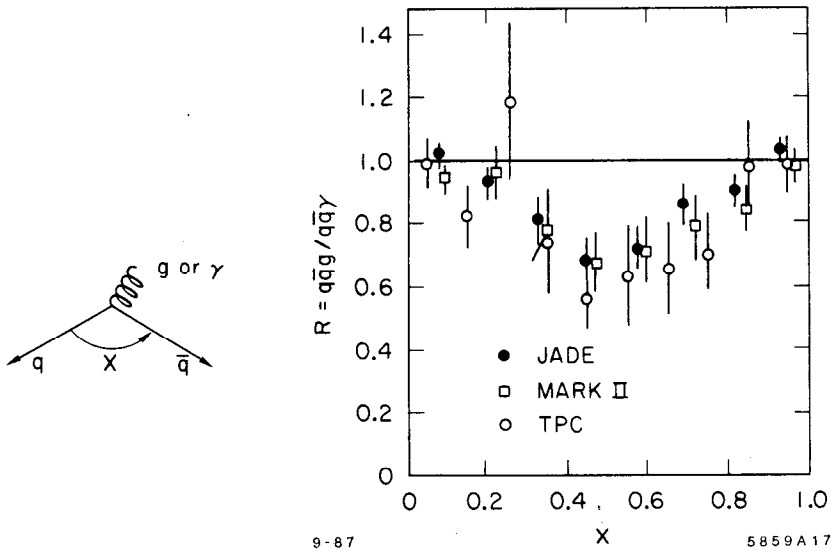

Fig. 19: The ratio of particle densities in $q\bar{q}g$ and $q\bar{q}\gamma$ events as function of the normalized angle $x = \phi/\phi_{q\bar{q}}$. The horizontal line at r=1 is the prediction if no interference effects occur in $q\bar{q}g$ events.

preferentially low momentum tracks in the 3-jet sample, so the effect is small. Disagreements at this level are also present in the LUND Monte Carlo up to $O(\alpha_s{}^2)$, e.g. in the 4-jet fraction of events[63] or the gluon fragmentation function[64].

Fig. 20a shows the fraction of multijet events as function of the jet resolution parameter from JADE data[63]. One sees that especially the 4-jet fraction is poorly described by the second order Monte Carlo. The shower Monte Carlos do a better job, but the leading log models shown do not reproduce the 3-jet cross section well for small invariant masses. This is remedied in the new LUND shower Monte Carlo, which incorporated the exact QCD matrix element for the radiation of the first gluon. In this case all the jet fractions are well described as shown by the preliminary TASSO data in Fig. 20b[65].

It was recently pointed out by Kramer and Lampe[44] that if one uses the PMS criterion (see Sect. 2.6) to find the optimum scale for the different multijet cross sections, the 4-jet rate comes out appreciably larger in the second order QCD calculations.

MARK-II[64] studied in a very nice way the properties of gluon jets by selecting symmetric 3-jet events ('MERCEDES' events) and determined the jet energies from the angles between the jets (see Eq. 43). Then they compare the momentum distribution of charged particles in these 3-jet events at 29 GeV with 2-jet events at 19 GeV. The average jet energies at 19 GeV are the same as the jet energies of the 2 quarks and gluon at 29 GeV. By taking the ratio of these distributions systematic effects largely cancel and one can compare a sample of 3-jet events, of which one is a gluon, with a sample of quark jets at the same averaged jet energy.

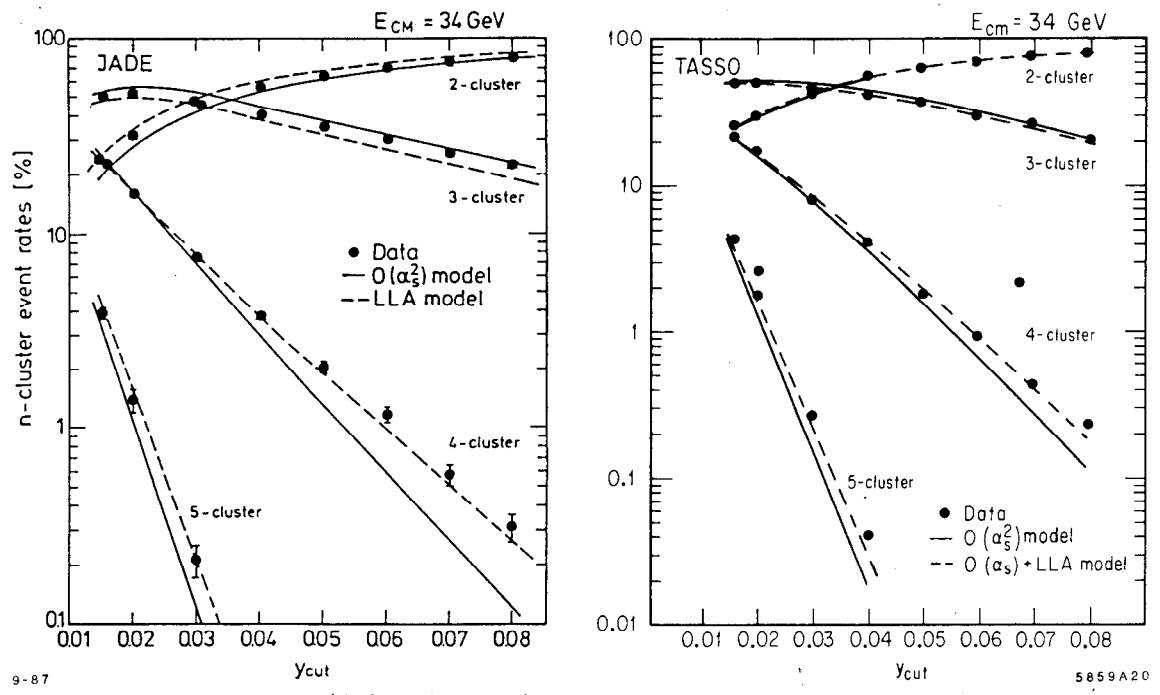

Fig. 20: The fraction of multijet events as function of the jet resolution (invariant jet mass y_{min}) compared with various models. Only the LUND shower model using the Leading Log Approximation for the shower cascade combined with the exact first order QCD matrix element for the first gluon can describe all jet multiplicities at the same time as shown by the curve $O(\alpha_s) + LLA$ through the preliminary TASSO data[65].

As can be seen from Fig. 21, this ratio is larger than one for small values of the scaled particle momentum $x_i = P_i/E_{jet}$, thus proving a softer distribution in the gluon enriched sample. A softer gluon fragmentation is expected in a non-abelian model, where the gluon carries colour. From the model predictions in Fig. 21 one sees that at high gluon momentum the spectrum of the LUND second order Monte Carlo is too hard; the shower models do reproduce the data better. JADE studied the transverse momentum of jets in 2- and 3-jet events and concluded that the transverse momentum is larger for gluon jets than for quark jets, indicating also a softer gluon fragmentation [66]. Recent summaries about the properties of gluon jets were given by Dorfan, Saxon and Sugano[1].

A recent comparison of the various Monte Carlo models with data at 29 GeV has been made by MARK-II[61]. They find that the LUND shower model using the correct $O(\alpha_s)$ matrix element for the first gluon and the leading log approximation for the soft gluons provides the most reasonable description of the data($\chi^2 \approx 2$ per point for 450 points), while the Webber shower Monte Carlo can be improved considerably if the phase space fragmentation of the clusters is replaced by string fragmentation. The Caltech-II Monte Carlo gives a considerably worse overall description of the data.

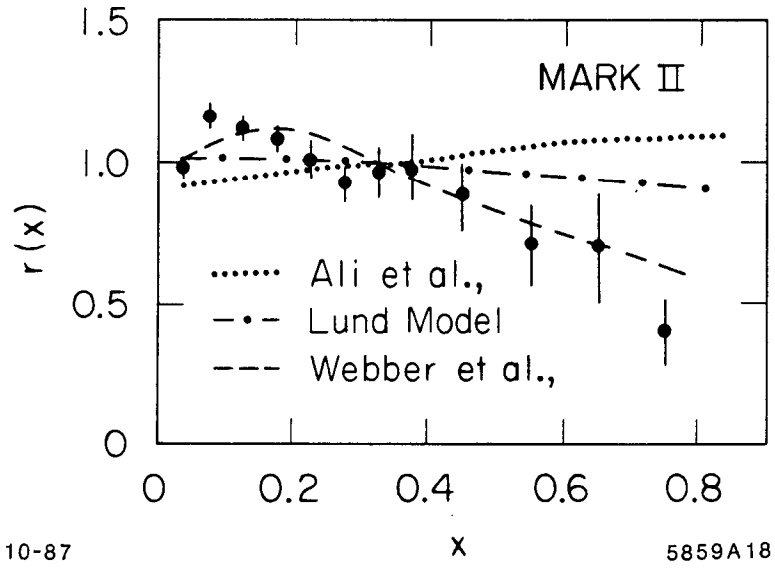

Fig. 21: The ratio of the inclusive charged particle distribution for three-fold symmetric 3-jet events at $\sqrt{s}$ = 29 GeV and 2-jet events at $\sqrt{s}$ = 19.3 GeV together with various model predictions.

5 Determination of α_s

Several methods have been used to determine the strong coupling constant α_s. Among them are:

- Event shape studies.
- Energy dependence of various quantities.
- Energy weighted angular correlations.
- Fits to the total hadronic cross section.

Here follows a summary of these results.

5.1 Shape variables

A study of variables which are sensitive to the event shapes or 'jettiness' can be used to determine the fraction of events with a hard gluon. Among the variables used are jet masses, sphericity, thrust, oblateness, and others or one uses cluster algorithms, which directly determine the number of 3-jet events. The problem with these variables is, that they are not only sensitive to α_s, but also to other 'knobs' in the Monte Carlo program, e.g. the transverse and longitudinal momentum spectra, the fraction of vector mesons etc. Therefore we will not consider these quantities further here.

5.2 Energy dependence

One can try to study the influence of fragmentation effects on α_s by determining the energy dependence of various quantities, since fragmentation effects will decrease with energy, while gluon radiation effects become more prominent as the energy increases. Such a study was first done by PLUTO[67]. However, the energy dependence is model dependent. Therefore it was suggested by Field[68] to use only the sign of the fragmentation effect and choose quantities for which the fragmentation is assumed to contribute either positively or negatively in the following way:

$$F = F_1 \left[\alpha_s(1 + C\alpha_s)\right] + F_2(fragmentation) \qquad (45)$$

Here F_1 is the known QCD prediction for the variable F, while F_2 represents the unknown fragmentation contribution. If one neglects F_2, one obtains an upper limit for α_s , if $F_2 > 0$ and a lower limit if $F_2 < 0$. Fig. 22a shows the α_s values from JADE[69] obtained from a fit of Eq. 45 to several variables and neglecting F_2. The variables studied are:

- The scaled average jet mass of the jet with the largest jet mass (M_h^2/E_{vis}^2). The heavy jet mass is proportional to α_s at the parton level and the coefficients have been calculated by Clavelli[70]. It can be seen that the fitted value of α_s from the jetmass decreases with energy as expected from the fact that fragmentation effects decrease with energy. Since all Monte Carlo models predict $F_2 < 0$, this variable can be used to obtain an upper limit (solid line). Since the energy dependence is not known, JADE did not make a fit to all points, but toke the best point (44 GeV), which gives a 95% C.L. upper limit on $\Lambda_{\overline{MS}}$ of 400 MeV.

- The thrust variable, plotted as $1 - T$, shows a similar behaviour, but gives less tight limits.

- The asymmetry of the energy weighted angular correlations (AEEC, see next Sect.), integrated between 45° and 90° is also shown in Fig. 22a. It shows little energy dependence.

For most models the AEEC has $F_2 < 0$, so it can be used to get a lower limit as shown by the $\Lambda = 25$ MeV curve in Fig. 22a. However, the sign of F_2 is not uniquely predicted: e.g. the Hoyer model gives $F_2 > 0$ for the integration range of 45° to 90°, so this model would give a somewhat lower Λ . However, the effect is small and if the integration range is enlarged, the sign of F_2 becomes also negative for the Hoyer model. This is the reason why CELLO[71] used an integration range between 30° and 90°. They fit the energy dependence of the scaled average heavy jet mass and the AEEC and find $\Lambda_{\overline{MS}}$ to be bound between 55 and 450 MeV at the 95 % C.L. The results are shown in Fig. 22b. The Λ limits given for both experiments correspond approximately to

$$\mathbf{0.10 < \alpha_s(1156\ GeV^2) < 0.16}$$

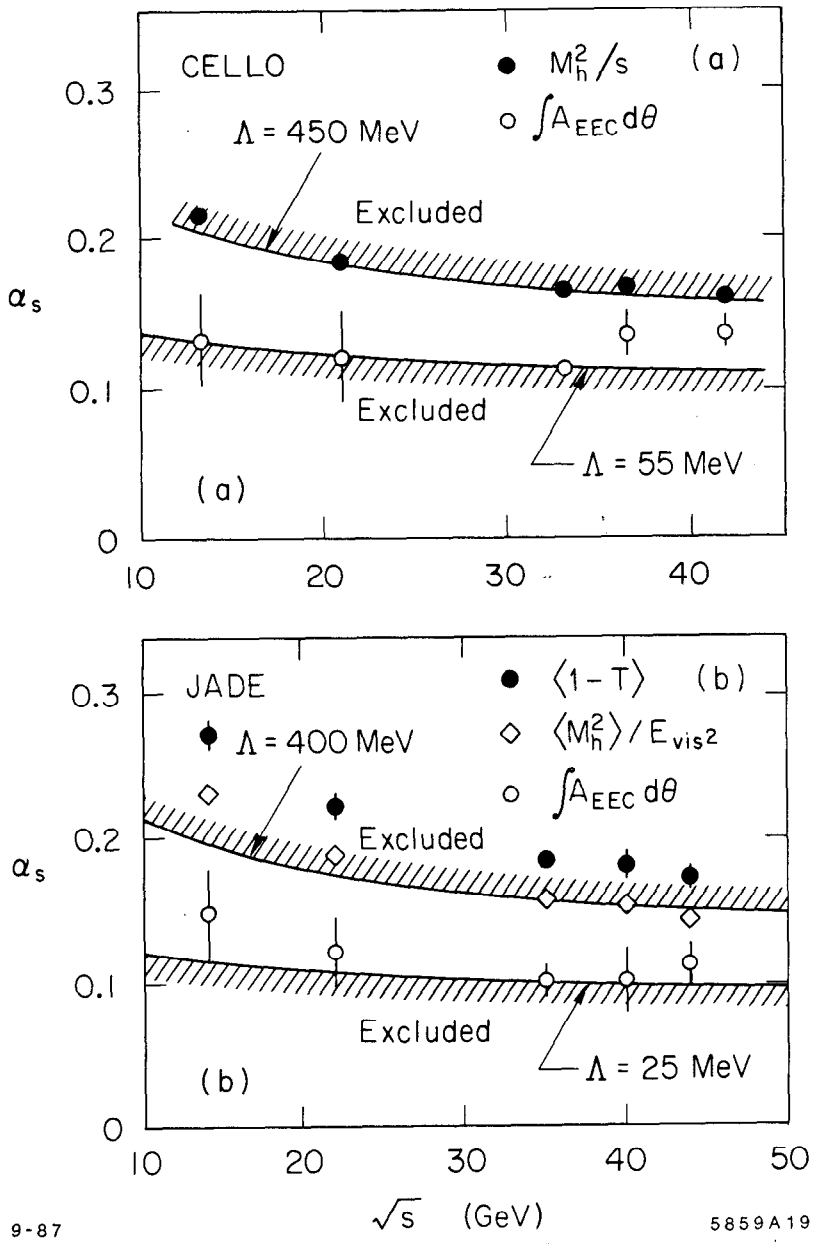

Fig. 22: Limits on α_s as function of centre of mass energy computed from various observables. Since the fragmentation term has been neglected, one gets lower limits from observables with a negative fragmentation contribution (AEEC) and upper limits from observables with a positive fragmentation contribution (M_h^2 and $1-T$). The error bars for the JADE data correspond to 2σ, so the solid lines drawn through the endpoints of the error bars of the 'best' point (the point at 44 GeV in this case) represent the 95% C.L. limit. The solid lines through the CELLO data represent the best fit of Eq. 45 with $F_2 = 0$. From the fitted values of α_s the indicated 95% C.L. limits on Λ were determined.

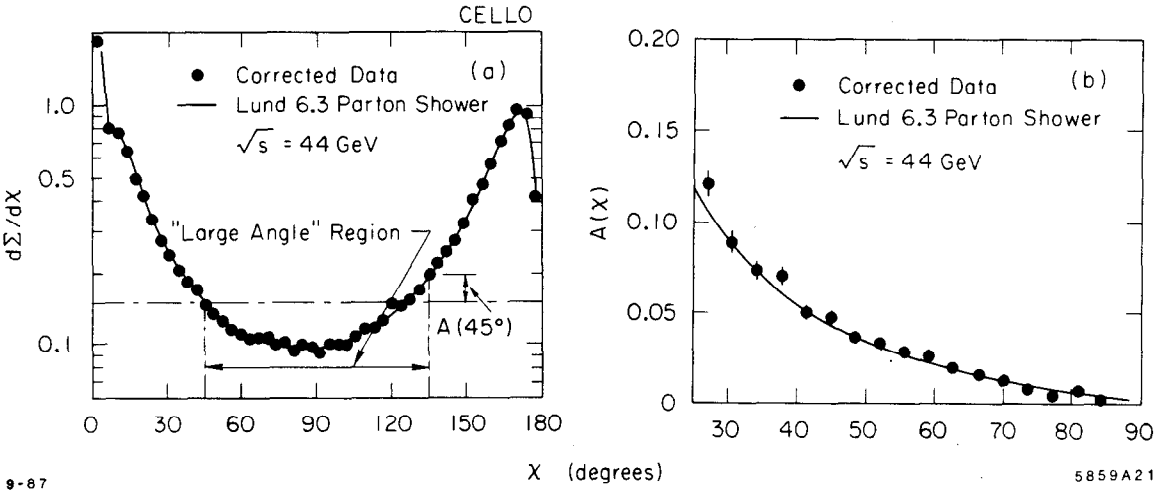

Fig. 23: An example of the energy-energy correlation (a) and asymmetry (b). The asymmetry $A(\chi)$ for 45°, defined as the difference between the EWAC at 135° and 45° is indicated in a).

5.3 Angular correlations

The energy weighted angular correlations (EWAC) were calculated first by Basham et al.[72] and later in higher order by other groups [73]. The way it is used by experimentalists, is simply producing a histogram of the angle χ_{ij} between any pair of particles or energy deposits in the detector with each entry weighted with the product of the two normalized energies of the pair.

An example of the normalized EWAC is shown in Fig. 23a. The two peaks near 0° and 180° show the predominant 2-jet character of the events: the peak near 0° corresponds to the small angles between the many particles within a jet, while the peak near 180° corresponds to the angles between particles belonging to opposite jets.

The EWAC distribution shows an asymmetry around 90° as shown e.g. for $\chi = 45°$ by the dashed lines in Fig. 23a. Such an asymmetry is not expected for 2-jet events, but 3-jet events automatically yield such an asymmetry, since a $q\bar{q}g$ event has usually one small angle and two large angles, so one gets more entries at the large angle side than at the small angle side. For $q\bar{q}$ events the asymmetry is negligible in the large angle region outside the cone of an average jet.

The determination of α_s from the asymmetry has several advantages:

- One can sum over all events, so no special jet axis determination or cluster algorithm has to be applied beforehand
- The AEEC has been calculated in $O(\alpha_s^2)$[73] and the second order corrections were found to be small at the parton level ($O(10\%)$).

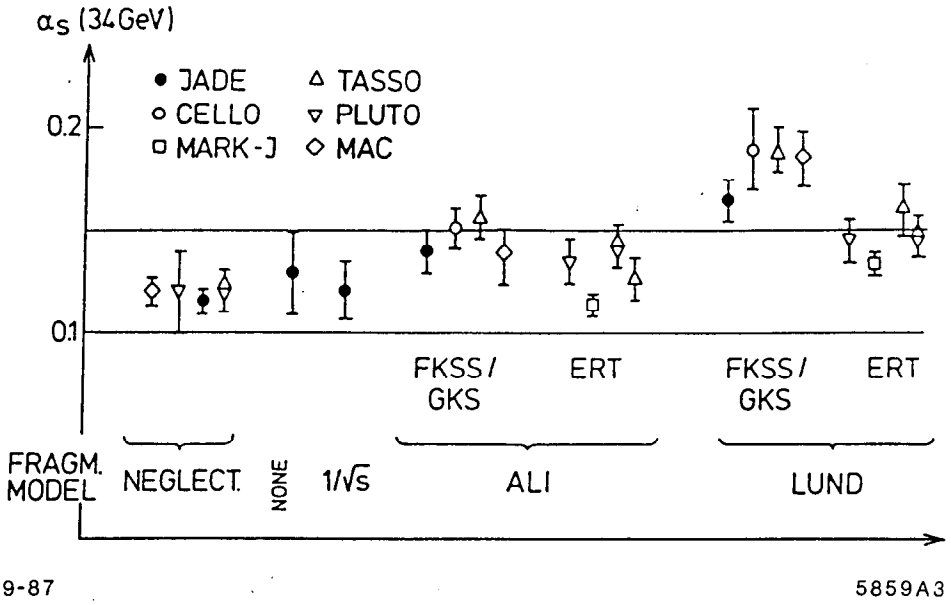

Fig. 24: A summary of the α_s values from the asymmetry in the energy energy correlations (see text).

- The energy weighting makes it an infrared stable quantity implying it to be insensitive to the specific cut-off parameters used to separate the 2-,3-, and 4-jet events.
- The contribution from $q\bar{q}$ fragmentation largely cancels in the asymmetry.

In spite of this impressive list of nice properties, the resulting α_s values found by the various groups still have a wide range of 0.12 to 0.19, as shown in Fig. 24[74]. The α_s values indicated as fragmentation models 'neglected' come from a fit of Eq. 45 with F_2=0, 'none' corresponds to the limits given in the previous section, and $1/\sqrt{s}$ assumes this energy dependence for F_2 in Eq. 45. The indication Ali+ERT corresponds to the Ali Monte Carlo with the ERT matrix element, while Ali+GKS corresponds to the independent fragmentation option in the Lund Monte Carlo.

For the LUND Monte Carlo the α_s values range from 0.14 to 0.19, if summed over the matrix elements. Since the ERT matrix element gives a larger 3-jet cross section than the GKS one (see Fig. 7 in Sect. 2.3), this spread is usually attributed to the different matrix elements. However, this conclusion is premature, since the AEEC is very similar for both matrix elements, at least if y-cuts are used, as shown before in Fig. 8. From this figure it is clear that the ERT matrix element actually gives a somewhat higher value of α_s , if one restricts the fits to the large angle range ($\cos\chi > -0.7$), since in this range ERT gives a lower parton asymmetry than GKS [3].

The differences are unlikely to originate from problems with the data, since in this case the values indicated as 'neglect' in Fig. 24 would show a similar

[3]An actual fit to the CELLO data with both matrix elements in this range yielded indeed a larger α_s value for ERT, but the difference is less than 0.002[75].

spread. Possible differences from the α_s values using the Lund model come from the different tuning and/or different versions of the Monte Carlos or the different range of χ used in the fit.

The influence of various fragmentation models on the AEEC has been summarized in Fig. 25 as function of α_s for $\sqrt{s} = 44$ GeV. The curves labeled Ali and Hoyer were generated with the options for independent fragmentation in the LUND program, so they all use the same GKS matrix element. It can be seen that the Hoyer model increases the asymmetry of the hadrons as compared to the parton asymmetry (line labeled partons), while the other models (Ali and LUND) decrease the asymmetry compared with the value at the parton level. Consequently, the observed asymmetry requires for the Hoyer model a lower value of α_s than for the Ali and LUND models. As can be seen from Fig. 25 from the averaged data at 44 GeV from CELLO[75], JADE[69] and TASSO[76] one finds:

$$\frac{\alpha_s{}^{Lund}}{\alpha_s{}^{Hoyer}} \approx 1.4 \tag{46}$$

while the ratio

$$\frac{\alpha_s{}^{Lund}}{\alpha_s{}^{Ali}} \approx 1.1 \tag{47}$$

is appreciably smaller.

The large difference between the two independent fragmentation models Ali and Hoyer comes mainly from the different mechanism of energy momentum conservation (EMC), as was first discovered by CELLO[77] and later studied in more detail by Sjöstrand[78]. In IF models the partons fragment independently, so energy and momentum cannot be conserved simultaneously, because one generates a massive jet from a massless parton. One then has to apply an EMC mechanism to the ensemble of the jets *after* fragmentation. The difference between Ali and Hoyer can be qualitatively explained as follows: The fragmentation of each parton is stopped below a certain energy, say 1 GeV. Then overal energy momentum conservation can be imposed in several ways:

- In Hoyer it is done by rescaling the jet energy of each jet separately in such a way that the jet directions are not changed, so the hadrons follow the original parton directions.
- In Ali it is done by performing first a boost in the direction of the missing momentum and then rescaling the energies.

For 2-jet events the effects are not important, since on the average the missing momemtum in opposite jets compensates. However, in case of 3-jet events, the missing momentum in the 2 opposite jets still compensates on the average, so the missing momentum tends to point in the direction of the third jet (usually the gluon jet). In the Hoyer case more energy is then given to the gluon to compensate the missing momentum, thus increasing the 3-jettiness. In the Ali case a boost is performed in the direction of the missing momentum, which is preferentially the

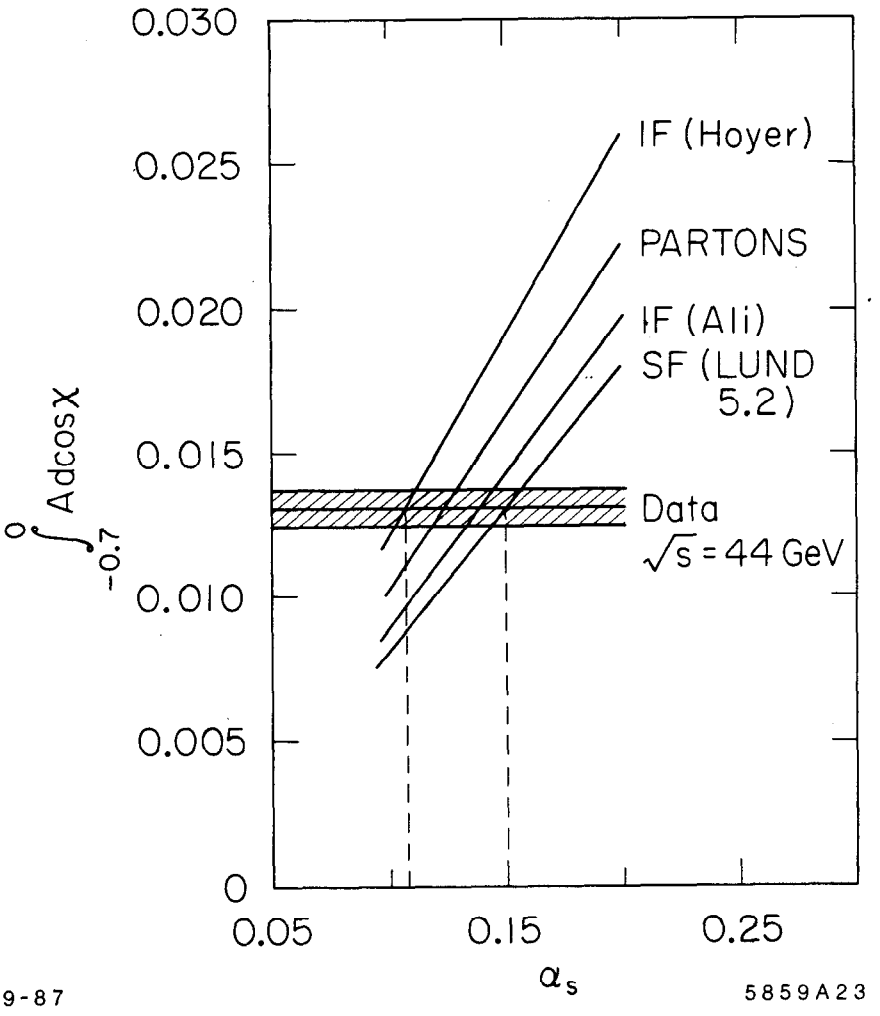

Fig. 25: Fragmentation model dependence of the integral of the AEEC as function of α_s. The curve labeled partons corresponds to the QCD prediction at the parton level. The other curves show the deviation after fragmentation for different models. The horizontal band indicates the averaged data from CELLO, JADE and TASSO at 44 GeV.

gluon. This has a similar effect as the boost of the strings in the LUND program, namely it decreases the average angle between the quark and gluon jet. Since the bremsstrahlung spectrum of the gluon is a steep function of this angle, one should not be surprised to find α_s to be sensitive to such effects in fragmentation models.

5.4 Conclusion on the asymmetry in angular correlations

What should be the conclusion of all this? Different collaborations give different answers. MARK-J[79] and PLUTO[80] maintain that one can determine α_s well from the AEEC. However, they estimate the systematic uncertainty from fragmentation models by cleverly picking the models which give very similar results: Ali and Lund, thus ignoring the Hoyer model.

JADE[81], MAC[82] and MARK-II[34] find a large difference in the α_s values between SF and IF models, but they find that IF models describe the data badly. However, this must be partly due to a poor tuning, since CELLO[77] and TASSO[33] find that their IF models describe the data reasonably well, at least in the angular range of interest [4].

The comparison of data with the Hoyer model is shown in Fig. 26 for CELLO and JADE data. JADE's tuning of the IF model disagrees everywhere, while the CELLO tuning of IF describes the data as well as SF in the angular range of interest (30° to 150°). The angles near 180° are not well described by the IF model, since $y_{min} = 0.03$ was used in that case, while for SF y_{min}=0.015 was used. The SF model would not describe the 'inside jet' region either with y_{min}=0.03[81].

However, it is difficult to use such a small y_{min} for the IF model, since in that case most events would have a soft gluon of a few GeV and IF models are not designed to fragment partons of a few GeV. The SF model has the nice property to absorb such soft gluons in the string, so their only effect is to generate some transverse momentum.

Note that even a small y_{min} of 0.015 eliminates already most angles below 20° at the parton level, so one should not be surprised to find disagreements in the 'inside jet' region at the hadron level. It is somehow fortuitous, that one can find a y_{min} for the SF model such that the 'hole' at the parton level is filled by the hadrons moved into this range by the string effect.

In conclusion, since all models can be tuned to describe the bulk of the data reasonably well, there seems to be no convincing arguments to eliminate some models in the estimate on the systematic uncertainties of α_s. Therefore, the uncertainty in α_s from fragmentation models is appreciably larger than the uncertainties from the different matrix elements and the different parton dressing schemes (see Sect. 2.3). Especially, the two most widely used matrix elements (ERT and GKS) give the

[4]One obvious difference between the tuning used by the different experiments is that JADE, MAC and MARK-II all use a very small y_{min} cut Of 0.015, while CELLO and TASSO use larger values. A y_{min} of 0.015 implies that most events have a gluon of a few GeV and fragmenting such low energy jets requires a delicate tuning. Furthermore, the last 2 experiments use the Petersen fragmentation function for heavy quarks, while the others use the LUND fragmentation function for heavy and light quarks, thus having less degrees of freedom.

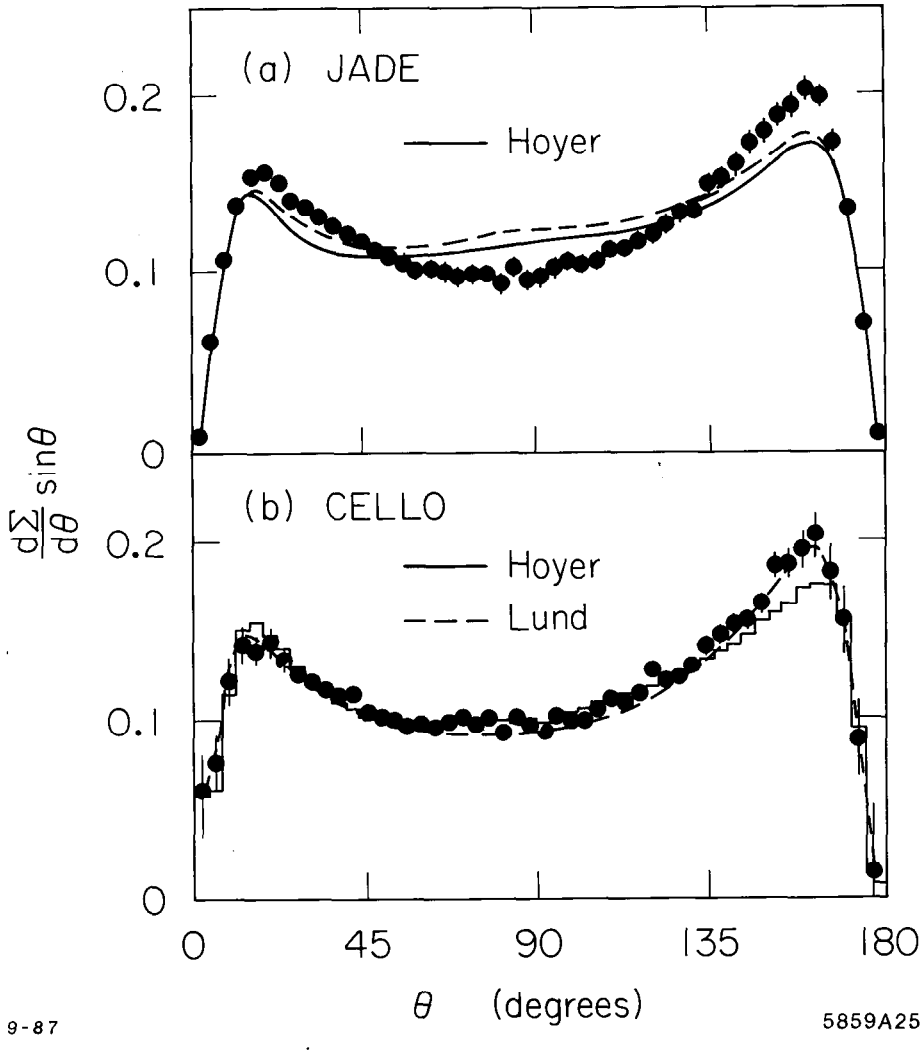

Fig. 26: Energy-energy correlation for different tunings of the Hoyer independent fragmentation model compared with JADE - (a) and CELLO data (b). The JADE figure at $\sqrt{s}$=34 GeV is from Ref.[81]. The solid and dashed curves represent the Monte Carlo with σ_q=210 MeV and 315 MeV, respectively. The main parameters of the Hoyer tuning describing the CELLO data at $\sqrt{s}$=44 GeV are: $\Lambda_{\overline{MS}}$=50 MeV; y_{min}=0.03; a=2.6 and b=1 in the Lund fragmentation function for light quarks, $\epsilon = 0.08$ and 0.015 in the Petersen fragmentation function for c and b quarks; the transverse momentum in a quark(gluon) jet is generated by a gaussian with a variance of σ =400(600) MeV.

same results for the AEEC in the large angle region, if y-cuts are used.

Considering the HOYER model and LUND model to be extremes, one finds from Fig. 25 for the α_s determinations at $\sqrt{s} = 44$ GeV:

$$\mathbf{0.11 < \alpha_s(1936\ GeV^2) < 0.16}$$

5.5 Triple energy correlations

Instead of angular correlations between 2 particles, Csikor et al.[83] proposed to use planar triple energy correlations (PTEC).

Obvious advantages are: a) One selects only planar particle combinations, thus one is able to suppress the contribution from multijet events. b) The acceptance corrections to the PTEC are less sensitive to the precise Monte Carlo tuning [84].

The PTEC was first studied by MARK-J[85] and recently also by CELLO[75]. The results have been summarized in Table 2. The α_s values are very similar to the ones from the AEEC; both matrix elements ERT and GKS give the same results (at least if y-cuts are used) and the fragmentation model dependence is as large as shown in Fig. 25 for the AEEC.

Experiment	Model	$\sqrt{s}$(GeV)	α_s
MARK J	Lund + ERT	35	0.147 ± 0.005
[85]	Ali + ERT	35	0.112 ± 0.005
CELLO	Lund + GKS	35	$0.151 \pm 0.003 \pm 0.006$
[75]	Lund + GKS	44	$0.145 \pm 0.004 \pm 0.006$
	Lund + ERT	44	$0.143 \pm 0.004 \pm 0.006$
	Hoyer + GKS	35	$0.103 \pm 0.002 \pm 0.006$
	Hoyer + GKS	44	$0.100 \pm 0.004 \pm 0.006$

Table 2: Summary of α_s values from planar triple energy correlations.

5.6 α_s from the total hadronic cross section

The fragmentation dependence of α_s as discussed above, does not occur in the α_s determination from R, since one needs Monte Carlos only to determine the acceptance of the detector (including radiative corrections), but not to determine the event shape. For 4π detectors the acceptance is not strongly dependent on the Monte Carlo model used. Furthermore, this determination of α_s is not plagued by theoretical uncertainties, 'higher twist' effects, large second order corrections, or a strong renormalization scheme dependence, which are among the caveats in other determinations of α_s as discussed in a very nice review by Duke and Roberts[41].

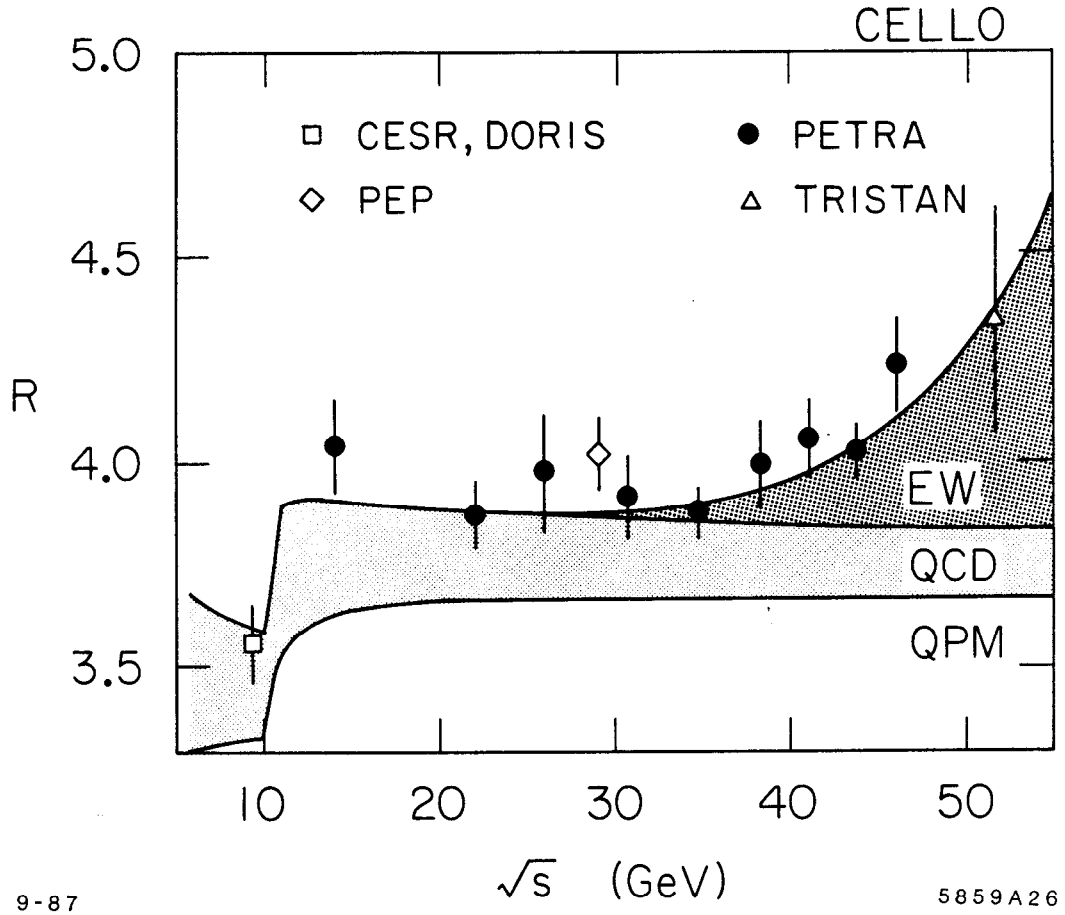

Fig. 27: R-values as function of centre of mass energy. The error bars include both systematic and statistical errors, which were obtained by combining the data in small intervals and fitting the averaged value, thus taking into account the correlations. The solid line is the result of the best fit with $\sin^2\theta_W$ =0.23.

The disadvantage is that the QCD contribution to R is only ≈5%, so one has to combine several experiments to get a good determination of R. In this case one has to study the systematic errors in detail. This was recently done by CELLO[39], who combined data from all experiments for $\sqrt{s}$ between 14 and 48 GeV and took the full error correlation matrix into account. More details about the method can be found in Ref.[86]. Fig. 27 shows an update of this analysis after including new data from TRISTAN at 50 and 52 GeV[87] and data below $\sqrt{s} < 10$ GeV[88]. The result of the fit is:

$$\alpha_s(1156\,\mathrm{GeV}^2) = 0.141 \pm 0.021 \text{ and } \sin^2\theta_W = 0.240 \pm 0.019$$

or

$$\Lambda_{\overline{MS}} = 245^{+250}_{-150}\mathrm{MeV}. .$$

This value of $\sin^2\theta_W$ is in good agreement with the world average of 0.23 [86]. We

used as additional input only G_F and α, so this value of $\sin^2\theta_W$ is determined only by the vector couplings of the quarks and has no large loop corrections, because of the Δr cancelations in Eq. 6. Since the quark couplings are apparently in agreement with the Standard Model expectations, we can keep $\sin^2\theta_W$ fixed at the world average of 0.23. Refitting yields:

$$\alpha_s(1156\ \mathrm{GeV}^2) = 0.145 \pm 0.019$$

or

$$\Lambda_{\overline{\mathrm{MS}}} = 290^{+230}_{-160}\mathrm{MeV}.$$

The value of α_s including the data around and below the Υ-region is somewhat lower than the result from the fit restricted to the energy above 10 GeV[39]. However, since the difference is within one standard deviation and both fits give an excellent χ^2 of about 0.7 per degree of freedom, there seems to be no reason to exclude part of the data.

Several points are worth mentioning:

- The result of the global fit describes well the single experiments. For example a fit of the normalization factor of each experiment was always compatible with the quoted normalization error.

- No correlations between different experiments were assumed, but the effect of an hypothetical common correlation error was estimated by introducing a correlated normalization error of 1% for all experiments in the full error correlation matrix. The effect on the fitted parameters was found to be small.

- Within one experiment, the measurements at different c.m. energies are certainly correlated. However, how much of the systematic error has to be considered common normalization error and how much point-to-point systematic error is not defined precisely. Therefore, the amount of splitting between normalization and point-to-point error was varied by $\pm 50\%$. The resulting change in the parameters is small as can be seen from the different error contours in Fig. 28.

  Note that these error contours correspond to $\chi^2_{min} + 1$. The extremes of the error contours, projected onto each axis correspond to $\pm 1\sigma$, i.e. 68% C.L. for each of the parameters (not to be confused with the C.L. inside the contour, which is 39% [47].)

- The value of α_s from R is in agreement with recent α_s values from deep inelastic scattering [89] and quarkonium decays[90] (see Table 3) and from limits on α_s presented in the previous section.

- The numerical value of α_s depends on the renormalization scheme. To give an experimental value of the QCD contribution independent of the renormalization scheme, it was fitted by a linear expression

$$R = R_{EW}\,(a + b(E - 34\mathrm{GeV})).$$

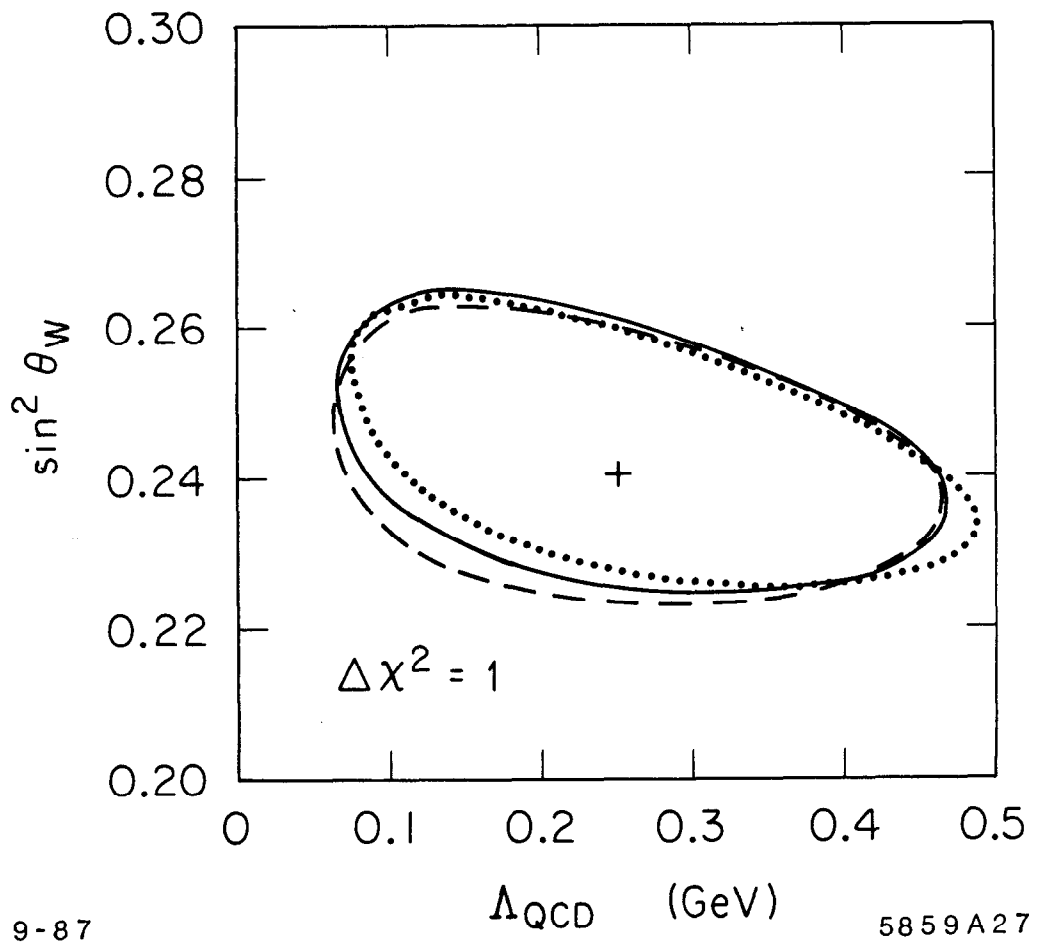

Fig. 28: Contour plots of α_s versus $\sin^2\theta_W$ for different assumptions on the splitting between systematic and point to point errors.

Here R_{EW} represents the electroweak contribution to R. For $\sin^2\theta_W$ =0.23 this yields $a = 1.060 \pm 0.011$ and $b = (-0.55 \pm 0.62)\ 10^{-3}\mathrm{GeV}^{-1}$. The term b gives a direct measurement of the running of the strong coupling constant. This result implies an 80% probability for α_s to run with a negative slope, and the absolute value is compatible with the one expected from QCD ($b = -1.3\ 10^{-3}\ \mathrm{GeV}^{-1}$) for $\alpha_s = 0.15$.

Recently JADE studied the energy dependence of the relative 3-jet rates, which was found to be in excellent agreement with the concept of a running coupling constant; they conclude that an energy independent coupling is unlikely[91].

From a study of the quarkonium annihilation rates, Kwong et al.[90] find the values of α_s at the charm and bottom mass are 0.29 ± 0.02 and 0.189 ± 0.009, respectively, if they assume the relativistic corrections vary in a linear fashion. Also the values in Table 3 are consistent with a running coupling constant.

Another way to argue that the coupling must be running is to say that we know confinement works, otherwise we would observe free quarks instead of jets of hadrons. The observation of confinement can be reconciled with the observation of a small coupling constant at high energies only, if the coupling constant is decreasing with increasing Q^2.

- The scale for α_s was chosen to be $Q = \sqrt{s}$. Changing scales is equivalent to changing renormalization schemes and uncertainties from this contribute only to $O({\alpha_s}^3)$, so these are expected to be negligible. The effect of different scales can be studied by choosing as scale $Q = x\sqrt{s}$ and using the modified formula for R (see Eqs. 35 and 36). For x between 0.5 and 1.5 the fitted value of α_s was found to vary less than $\pm 4\%$ (as expected from Fig. 10), so this is small compared with the total systematic error of 15%, which is dominated by the systematic uncertainties in the R measurements.

- Note that the quoted Λ value is the one for 5 flavours, even although one includes also data below $b\bar{b}$ threshold. This is consistent with the $\overline{MS}$ prescription, that N_f should be changed at $Q = m_q$ and not at $Q = 2m_q$[38]. Nevertheless, if one chooses a different scale, say $\sqrt{s}/2$, one comes in the range where $N_f = 4$. If one fits Λ one has to use in this region the more complicated formula for α_s (see Eq. 25), which takes into account that the value of α_s does not change if one passes a new threshold, but only the running becomes slower, if N_f increases (it becomes ≈ 0 for N_f=16). Since the running of α_s does not change strongly by going from $N_f = 5$ to $N_f = 4$ in the small energy range below 10 GeV, this is a negligible effect as was checked from actual fits.

- The experimental data has not been corrected for more than one photon radiated in the initial state, since these calculations have become available only recently [92]. Previously the effect was estimated to be at the % level and a reduction of all R-values by 1% would reduce α_s by 15%[39]. However,

a preliminary estimate with the exact calculations indicates that the effect is appreciably smaller, since the radiative corrections are only important at high energies, so it lowers $\sin^2\theta_W$ somewhat, but hardly changes α_s. More definite statements require a Monte Carlo simulation, because the higher order corrections depend on the maximum allowed photon energy.

Process	Q	N_f	α_s	$\Lambda_{\overline{MS}}$(GeV)
$\frac{\Gamma(\Upsilon\to\gamma gg)}{\Gamma(\Upsilon\to ggg)}$[90]	5	4	$0.180^{+0.009}_{-0.008}$	$0.182^{+0.033}_{-0.032}$
deep inel. μC[89]	10	4	$0.160 \pm 0.003 \pm 0.01$	$0.230 \pm 0.020 \pm 0.060$
$R(e^+e^-)$	34	5	0.141 ± 0.021	$0.245^{+0.250}_{-0.150}$

Table 3: Comparison of a few recent α_s values in different processes at different values of Q^2 (Q in GeV). The $\Lambda_{\overline{MS}}$ value from R was calculated for 5 flavours. The other $\Lambda_{\overline{MS}}$ values were calculated for $N_f = 4$, which can be compared with the value for five flavours by multiplying them by ≈0.7 (see Eq. 26). Note that all Λ values are based on Eq. 24 and not on Eq. 23, which would give a ≈15% lower value. A compilation of older or more debatable α_s determinations can be found in Refs.[41,89,90] and Sect. 5 of this report.

6 Conclusion

Comparing our present knowledge about QCD with what was known some 10 years ago, it is fair to say that we learned a lot from PEP and PETRA physics, namely:

- At high energies partons become observable as jets on an event by event basis, thus starting the era of studying *parton dynamics* instead of *particle dynamics.*
- First evidence for gluons came from the observation of clear 3-jet events. This unexpected discovery of the 'heart' of QCD is of equal importance as the discovery of the carriers of the weak force, namely the W and Z bosons.
- From angular distributions quarks were found to be spin 1/2 particles and gluons to be spin 1 particles, as expected for matterfields and gauge bosons in the Standard Model.
- From the total hadronic cross section one observes:
  - Quarks come in 3 colours and their electric charges agree with the standard fractional charge assignments.

- A clear contribution from the direct Z^0-exchange is observed at the highest energies ($40 < \sqrt{s} < 52$ GeV).
- A fit to the hadron cross section data above $\sqrt{s}$=8 GeV yields:

$$\alpha_s(1156\,\mathrm{GeV}^2) = 0.141 \pm 0.021 \text{ and } \sin^2\theta_W = 0.240 \pm 0.019$$

- The scale (or renormalization scheme) dependence of the α_s determination from R was studied in detail and found to be of the order of a few %, which is small compared with the total experimental error of 15%. Also the sensitivity to the number of flavours used in the formula for α_s was found to be small, as long as care was taken that only the running of α_s could change for a different number of flavours, not is value (see Eqs. 25 and 26).
- The couplings of quarks to the Z^0 are in agreement with the Standard Model expectations, as is apparent from the above value of $\sin^2\theta_W$, which is completely determined by the vector couplings of the quarks to the Z^0 with the parametrization of the cross section in terms of G_F (see Eq. 6).

- Several observations (R, observation of jets, 3-jet rates, and quarkonium annihilation rates, see previous Section) indicate that α_s is decreasing with increasing Q^2, as expected if the gluon carries colour itself, thus leading to diagrams with gluon self-coupling as shown in Fig. 3b.

Although several features of QCD remain to be tested, like e.g. the observation of glue-balls (bound gluon states), I believe that the discovery of the gluon and the fact that QCD is able to provide a consistent picture for all the features mentioned before, has promoted it from the 'candidate' theory, which it was 10 years ago, to the only acceptable theory of the strong interactions.

Acknowledgements

Many thanks go to Therese Tymienicka and the Organizers of this Conference for inviting me to such a pleasant place.

I wish to thank my colleagues at PEP and PETRA for providing me their latest results, especially Andreas Dieckman, Klaus Gamerdinger, Jochen Hansmeyer, Luis Labarga, and F. Ould-Saada.

Thanks also to Gerrit Burgers for providing a program to calculate the second order radiative corrections, to Giulio D'Agostini, Günter Grindhammer and Wolfgang Hollik for the many stimulating discussions and to Siegfried Bethke, Jonathan Dorfan and Luis Labarga for their comments on the manuscript.

I thank the SLAC Directorate for the hospitality I am enjoying at SLAC and last but not least I want to thank my wife and children for their patience during the time of writing this review, which coincided with the time of moving to another continent.

References

[1] P. Söding and G. Wolf, Ann. Rev. Nucl. Sci. **31**(1981) 231
Sau Lan Wu, Phys. Rep. **107**(1984) 59
H. Yamamoto, Proc. of 1985 SLAC Summer Inst. Stanford (1985)
F. Barreiro, Fortschr. Phys. **34** (1986) 503
D.H. Saxon, Int. School of High Energy Phys., Duilovo-Split, Yugoslavia, (1986), RAL-86-057
W. de Boer, Proc. of 17th Int. Symp. on Multiparticle Dyn., Seewinkel, Austria (1986); MPI-PAE/Exp.El. 167
J. Dorfan, Proc. of 1986 SLAC Summer Inst., Stanford (1986)
K. Sugano, Proc. of Phys. in Collision VI, Chicago (1986)
P. Mättig, DESY Report 86-161, Cracow School of Theor. Phys., Zakopane, Poland, 1986
J. Chrin, DESY Report 87-040

[2] Details and ref. can be found in standard text books:
F.E. Close, An Introduction to Quarks and Partons, Academic Press (1979)
L.B. Okun, Leptons and Quarks, Noth Holland Publ. Comp. (1982)
K. Huang, Quarks, Leptons and Gauge Fields, World Scientific, (1982)
C. Quigg, Gauge Theories of the strong, weak and electromagnetic Forces, Benjamin-Cummings Publ. Comp. Inc. (1983)
J.E. Dodd, The ideas of Particle Physics, Cambridge Univ. Press (1984)
F. Halzen and A.D. Martin, Quarks and Leptons, An introductory course in Modern Particle Physics, John Wiley and Sons, Inc. (1984)
D.H. Perkins, Introduction to High Energy Physics, Addison Wesley Publ. Comp. (1987)

[3] H. Fritzsch and M. Gell-Mann, 16th Int. Conf. on High Energy Physics, Chicago (1972)
H. Fritzsch, M. Gell-Mann and H. Leutwyler, Phys. Lett. **47B** (1973) 365

[4] D.J. Gross and F. Wilczek, Phys. Rev. Lett. **30** (1973) 1343

[5] H.D. Politzer, Phys. Rev. Lett. **30** (1973) 1346

[6] G.S. Abrams et al., Phys. Rev. Lett. **33** (1974) 1452

[7] J.J. Aubert et al., Phys. Rev. Lett. **33** (1974) 1404

[8] M. Gell-Mann, Phys. Lett. **8** (1964) 214

[9] G. Zweig, CERN report 8419TH 412 (1964)

[10] S.L. Glashow, Nucl. Phys. **22** (1961) 579; Rev. Mod. Phys. 52 (1980) 539
S. Weinberg, Phys. Rev. Lett. **19** (1967) 1264; Rev. Mod. Phys. 52 (1980) 515
A. Salam, Rev. Mod. Phys. 52 (1980) 525
For an historical account, see S. Coleman, Science **206** (1979) 1290

[11] G. 't Hooft, Nucl. Phys. **B 35** (1971) 167

[12] S.L. Glashow, J. Iliopoulos and L. Maiani, Phys. Rev. **D2** (1970) 1285

[13] S.W. Herb et al., Phys. Rev. Lett. **39** (1977) 252

[14] M. Perl et al., Phys. Rev. Lett. **35** (1975) 1489; Phys. Lett. **63B** (1976) 366

[15] J. Ellis, M.K. Gaillard, and G.G. Ross, Nucl. Phys. **B111** (1976) 253; ibid. **B130** (1977) 516;

[16] Mark-I Coll., G. Hanson et al., Phys. Rev. Lett. **35** (1975) 1609

[17] A. Sirlin, Phys. Rev. **D22** (1980) 891
W.J. Marciano and A. Sirlin, Phys. Rev. **D29** (1984) 945

[18] W. Hollik, DESY Report 86-049, Proc. 21st Renc. de Moriond. Les Arcs, France (1986)
M. Böhm et al., Fortsch. Phys. **34** (1986) 687

[19] A. Barroso et al., CERN-EP/87-70, presented by F. Dydak at LEP200 ECFA Workshop, Aachen (1986)
J.P. Alexander et al., SLAC-PUB-4376, submitted to Phys. Rev.

[20] T. Kinoshita, J. Math. Phys. **3** (1962) 650
T.D. Lee and M. Nauenberg Phys. Rev. **D133** (1964) 1549

[21] G. Kramer and B. Lampe, DESY Reports 86-103 and 86-119

[22] A. Ali et al., Nucl. Phys. **B167** (1980) 454; Phys. Lett. **82B** (1979) 285
J.G. Körner et al., Nucl. Phys. **B185** (1981) 365
K.J.F. Gaemers and J.A.M. Vermaseren, Z. Phys. **C7** (1980) 81
O. Nachtmann and A. Reiter, Z. Phys. **C14** (1982) 47; ibid. **C16** (1982) 45

[23] F. Gutbrod, G. Kramer, G. Schierholz, Z. Phys. **C22** (1984) 235

[24] R.K. Ellis, D.A. Ross, E.A. Terrano, Phys. Rev. Lett. **45** (1980) 1225;
Nucl. Phys. **B178** (1981) 421

[25] J.A.M. Vermaseren, K.J.F. Gaemers, S.J. Oldham, Nucl. Phys. **B187** (1981) 301

[26] T.D. Gottschalk, Phys. Lett. **109B** (1982) 331
T.D. Gottschalk and M.P. Shatz, CALT-68-1172,-1173,-1199; Phys. Lett. **150B** (1985) 451

[27] G. Kramer, DESY Report T-83-01 and Theory of Jets in Electron-Positron Annihilation, Springer Tracts in Modern Physics, Vol. 102 (1984)

[28] R.Y. Zhu, Ph. D. Thesis, MIT (1983)

[29] A. Ali, Phys. Lett **110B** (1982) 67

[30] Z. Kunszt, Phys. Lett. **99B** (1981) 429; ibid. **107B** (1981) 123

[31] F. Csikor, private communication

[32] G. Rudolph, Habilitationsschrift, Innsbruck (1986)
F. Gutbrod et al., DESY Report 87-047

[33] TASSO Coll., M. Althoff et al., Z. Phys **C26** (1984) 157

[34] MARK-II Coll., D.R. Wood et al., SLAC-PUB 4374, to be published

[35] G. 't Hooft and M. Veltman, Nucl. Phys. **B44** (1972) 189

[36] O. Tarasov, A. Vladimirov, and A. Zharkov, Phys. Lett. **93B**(1980)429

[37] Particle Data Group, M. Aguilar-Benitez et al., Phys. Lett. **B170** (1986) 78

[38] W.J. Marciano, Phys. Rev. Lett. **29** (1983) 580

[39] CELLO Coll., H.J. Behrend et al., Phys. Lett. **B183** (1987) 400

[40] M. Dine, J. Sapirstein, Phys. Rev. Lett. **43** (1979) 668
K.G. Chetyrkin et al., Phys. Lett. **B85** (1979) 277
W. Celmaster, R.J. Gonsalves, Phys. Rev. Lett. **44** (1979) 560

[41] D.W. Duke, R.G. Roberts, Phys. Reports **120** (1985) 275

[42] P.M. Stevenson, Phys. Rev. **D23** (1981) 2916

[43] G. Grindhammer, F. LeDiberder and J. Haissinski, CELLO Note O-83

[44] G. Kramer and B. Lampe, DESY Report 87-106

[45] W. Celmaster and R.J. Gonsalves, Phys. Rev. **D20** (1979) 1420; Phys. Rev. Lett. (**42** (1979) 1435

[46] S. Brodsky, G.P. Lepage and P. Mackenzie, Phys. Rev. **D28** (1983) 493

[47] R. Marshall, RAL-87-031 (1987)

[48] U. Amaldi et al., UPR-0331T (1987)

[49] B. Andersen et al. Phys. Rep. **97** (1983) 31
T. Sjöstrand, Computer Phys. Comm. **27** (1986) 243
T. Sjöstrand, Computer Phys. Comm. **28** (1986) 229
T. Sjöstrand, Computer Phys. Comm. **39** (1986) 347
T. Sjöstrand and M. Bengtsson, Computer Phys. Comm. **43** (1987) 367

[50] J. Ellis and I. Karliner, Nucl. Phys. **B148** (1979) 141

[51] TASSO Coll., R. Brandelik et al. Phys. Lett. **97B** (1980) 453

[52] CELLO Coll., H.J. Behrend et al. Phys. Lett. **110B** (1982) 329
JADE Coll., W. Bartel et al. Phys. Lett. **119B** (1982) 239
PLUTO Coll., Ch. Berger et al., Phys. Lett. **97B** (1980) 459
P. Söding, AIP Conf. Proc., APS-meeting, Santa Cruz (1981)

[53] R. D. Field and R.P. Feynman, Nucl. Phys. **B136** (1978) 1

[54] P. Hoyer et al., Nucl. Phys. **B161** (1979) 349

[55] A. Ali et al. Phys. Lett. **93B** (1980) 155

[56] T.D. Gottschalk, Nucl. Phys. **B214** (1983) 201; ibid **B239** (1984) 349
T.D. Gottschalk and D. Morris, Nucl. Phys. **B288** (1987) 729

[57] G. Marchesini and B.R. Webber, Nucl. Phys. **B238** (1984) 1

[58] JADE Coll. W. Bartel et al., Z. Phys. **C21** (1983);
Phys. Lett. **134B** (1984) 275; ibid. **157B** (1985) 340
TPC Coll., M. Aihara et al., Z. Phys. **C28** (1985) 31
TASSO Coll., M. Althoff et al., Z. Phys. **C29** (1985) 29

[59] Y.I. Azimov et al., Phys. Lett. **165B** (1985) 147

[60] M. Bengtsson and T. Sjöstrand, Nucl. Phys. **B289**(1987)810

[61] MARK-II Coll., A. Petersen et al., SLAC-PUB-4290, submitted to Phys. Rev. D

[62] TPC Coll., M. Aihara et al.,Phys. Rev. Lett. **57** (1986) 945
MARK-II Coll., P. Sheldon et al.,Phys. Rev. Lett. **57** (1986) 1398
JADE Coll., W. Bartel et al., Contr. to Int. Symp. on Lepton and Photon Int., Hamburg (1987)

[63] JADE Coll., W. Bartel et al., Z. Phys. **C33** (1986) 23

[64] MARK-II Coll., A. Petersen et al., Phys. Rev. Lett. **55** (1985) 1954

[65] TASSO Coll., Contr. to Int. Symp. on Lepton and Photon Int., Hamburg (1987)

[66] JADE Coll., W. Bartel et al., Phys. Lett. **123B** (1983) 460

[67] PLUTO Coll., Ch. Berger et al., Z. Phys. **C12**(1981) 297

[68] R.D. Field, Proc. Int. Symp. on Lepton and Photon Int., Cornell (1983)

[69] A. Dieckmann, Ph.D. thesis, Heidelberg (1987)

[70] L. Clavelli and D. Wyler, Phys. Lett. **103B** (1981) 383

[71] J. Hansmeyer, Ph.D. thesis, Karlsruhe (1987)

[72] C.L. Basham et al., Phys. Rev. **D17**(1978)2298

[73] A. Ali and F.Barreiro, Phys. Lett **118B** (1982) 155; Nucl. Phys. **B236** (1984) 269
D.G. Richards, W.J. Stirling, Nucl. Phys. **B229** (1983) 317

[74] S. Bethke, Proc. of 23th Conf. on High Energy Phys., Berkeley (1986)
B. Naroska, Phys. Rep. **148** (1987) 67

[75] K. Gamerdinger, Ph.D. thesis, Karlsruhe, in preparation

[76] TASSO Coll., W. Braunschweig et al., DESY Report 87-081

[77] CELLO Coll. H.J. Behrend et al., Nucl. Phys. **B218** (1983) 269;
Phys.lett. **138B** (1984) 311

[78] T. Sjöstrand, Z. Phys. **C26** (1984) 93

[79] MARK-J Coll., B. Adeva et al., Phys. Rev. Lett.**54** (1985) 1750

[80] PLUTO Coll., Ch. Berger et al., Z. Phys. **C28** (1985) 365

[81] JADE Coll., W. Bartel et al., Z. Phys. **C25** (1984) 231

[82] MAC Coll., E. Fernandez et al., Phys. Rev. **D31** (1985) 2724

[83] F. Csikor et al., Phys. Rev. **D31** (1985) 1025

[84] M. Chen and L. Garrido, Phys. Lett. **180B** (1986) 409

[85] MARK-J Coll., B. Adeva et al., Phys. Lett. **180B** (1986) 181

[86] W. de Boer, Proc. of 17th Int. Symp. on Multiparticle Dyn., Seewinkel, Austria (1986);
MPI-PAE/Exp.El. 167
G. D'Agostini, Proc. of Renc. de Moriond, (1987) to be published

[87] Results on R from the AMY-, TOPAZ- and VENUS-Coll. were presented by S. Ozaki at the Int. Symp. on Lepton and Photon Interactions, Hamburg (1987)

[88] Crystal Ball Coll., Int. Symp. on Lepton and Photon Interactions, Hamburg (1987)
CLEO Coll., R. Giles et al., Phys. Rev. **D29** (1984) 1285
CUSB Coll., E. Rice, Ph. D. thesis, Columbia University (1982)
DASP2 Coll., S. Weseler, Diploma thesis, University of Heidelberg (1981)
DASP2 Coll., H. Albrecht et al., DESY Report 82-037 (1982), unpublished
DESY-Hamburg-Heidelberg-MPI Munich Coll., P. Bock et al., Z. Physik **C6** (1980) 125
LENA Coll., B. Niczyporuk et al., Z. Physik **C15** (1982) 299
PLUTO Coll., L.Criegee and G. Knies, Phys. Rep. **83** (1982) 151

[89] A.C. Benvenuti et al., CERN-EP/87-101, submitted to Phys. Lett. B

[90] W. Kwong, P.B. Mackenzie, R. Rosenfeld and J.L. Rosner, EFI 87-31, Chicago, 1987

[91] JADE Coll., Int. Symp. on Lepton and Photon Interactions, Hamburg (1987)

[92] F.A. Berends, G.J.H. Burgers and W.L. van Neerven, Phys. Lett. **185B** (1987) 395